Electronic Supplementary Material (ESI) for Energy & Environmental Science.

Combined, time-resolved, *in situ* neutron reflectometry and *x*-ray diffraction analysis of SEI formation under dynamic current conditions for electrochemical N_2 reduction – Supporting Information

Sarah J. Blair[†a,c], Mathieu Doucet*[†b], Valerie A. Niemann[a,c], Kevin H. Stone[d], Melissa E. Kreider[a,c], James F. Browning[b], Candice E. Halbert[b], Hanyu Wang[e], Peter Benedek[a,c], Eric J. McShane[a], Adam C. Nielander*[c], Alessandro Gallo*[c], Thomas F. Jaramillo*[a,c]

[1]Department of Chemical Engineering, Stanford University, Stanford, CA 94305, United States

[2]Neutron Scattering Division, Oak Ridge National Laboratory, Oak Ridge, TN 37831, United States

[3]SUNCAT Center for Interface Science and Catalysis, SLAC National Accelerator Laboratory, 2575 Sand Hill Road, Menlo Park, CA 94025, United States

[4]Center for Nanophase Materials Sciences, Oak Ridge National Laboratory, Oak Ridge, TN 37831, United States

[†]These authors contributed equally to this work.

*Corresponding author

Thin Film Synthesis for Neutron Reflectometry Samples

Molybdenum and Pt thin films were prepared using a custom-built electron-beam physical vapor deposition (PVD) system (Technical Engineering Services). For Mo samples, Si wafers that were 2 inches in diameter and 5 mm in thickness (Institute of Electronic Material Technology, n-type, Si:P[111], Ro > 20 ohm-cm) were sonicated in 5:4:1 deionized water (18 MΩ cm): isopropanol: acetone, rinsed in deionized water, and dried using compressed nitrogen prior to deposition. 50-nm Mo films were then deposited directly onto the Si wafers at a deposition rate of 0.2 Å/s using a Mo source target as received (Mo, 99.95% purity, Kurt J. Lesker). Larger Si wafers (2 inches in diameter, 10 mm in thickness) with two holes drilled into the wafer for filling of the cell were cleaned as described above and used as substrates for Pt deposition. 100-nm Pt films were deposited at a rate of 1 Å/s onto a 3-nm Ti sticking layer (deposited at a rate of 0.5 Å/s) directly atop these substrates using metal source targets as received (Ti, 99.995%; Pt, 99.99% purity, Kurt J. Lesker).

X-Ray Photoelectron Spectroscopy

A PHI III Versaprobe equipped with Al Kα radiation (1486 eV) was used to perform XPS on representative samples. High-resolution spectra were measured using a pass energy of 55 eV with a 200 µm spot size. Depth profiles were measured via sputtering using an Ar gun at a sputtering rate of 3 nm/min. Using CasaXPS software, spectra were aligned by setting the high-resolution scan of the C 1s peak to 284.8 eV. A Shirley background was used to fit peaks.

Electrolyte Preparation for Neutron Reflectometry Measurements

The electrolyte was composed of d_8-THF (Sigma-Aldrich, Inc.), 0.2 M $LiClO_4$ (battery-grade, dry, 99.99% trace metals basis, Sigma-Aldrich, Inc.), with or without 0.17 M ethanol (Sigma-Aldrich, 200 proof, anhydrous, ≥99.5%) and was mixed in an Ar glovebox (2-3 ppm O_2). Five mL of electrolyte were then sparged in a custom glass sparging cell with N_2 (99.999% UHP, Praxair) for 15 minutes. The gases were first passed through a NuPure gas purifier (Eliminator Model 40 PF) and subsequently bubbled into a Pyrex bottle containing dry tetrahydrofuran (Sigma-Aldrich, Inc., anhydrous, inhibitor-free, 99.9%) before passing into the electrolyte vessel in order to pre-saturate the gas with solvent to prevent electrolyte evaporation during sparging. Figure S2 depicts the setup.

Electrochemical Cell Preparation

Ag paint (PELCO conductive silver paint, Ted Pella, Inc.) was painted onto the edges of the electrode films for electrical contact such that the paint would be outside of the O-ring and would not come into contact with electrolyte. Cu tape was then taped onto the sides of the electrodes on top of the paint to facilitate electrical contact of the cell screws with the metallic electrode films. The electrochemical cell was then assembled, leaving the electrolyte ports unplugged, and brought into the Ar glovebox. Using a glass syringe, the electrolyte was removed from the glass sparging vessel through a septum and introduced into the electrochemical cell via the Teflon Luer fitting screwed into a cell port. When the cell was filled with electrolyte, a leakless PEEK Ag/AgCl reference electrode (eDAQ, Model ET072 or Innovative Instruments, LF-1.6-35) was inserted into

the second port and tightened using a PEEK IDEX fitting with a ferrule or O-ring. The Luer fitting port was plugged using a Teflon plug, and both ports were wrapped in Parafilm. The cell was then transported to the Beamline 4B Liquids Reflectometer (LR) station.

Time-Resolved Data Processing for Neutron Reflectometry

The models obtained for the steady-state reflectivity data were used as initial models for the time-resolved data. The initial OCP model (labelled "pre cycle 1" in the main text), was used as the initial model for the constant current data of the first cycle. The Mo layer and the SLD of the electrolyte were kept fixed and only Layer 1 was used until the 30-second mark, after which the Mo needed to vary and Layer 2 added. The same approach was used for the constant-current data of cycle 2. In this case, the "post cycle 1" OCP model was used as the initial model, and Layer 2 was added at the 15-second mark. The post cycle 1 model to which Layer 2 was added was used for the return to OCP data of cycle 1.

The fitting engine used for modeling was the DREAM algorithm[1] implemented in refl1d. This algorithm uses a Markov Chain Monte Carlo (MCMC) method to sample the posterior probability distribution of the models, which can be used to assess the uncertainty on the parameters. Similarly, one can get information about the range of likely SLD values as a function of depth. The probability distribution of the SLD as a function of depth was assessed by computing the SLD value at each z for each solution of the Markov chain and subsequently calculating the two-sided 90% confidence level (90% CL) interval for each z value. The 90% CL intervals are shown on the SLD figures. It should be noted that the plotted SLD profiles correspond to the best model found for a given measurement, which does not necessarily correspond to the middle of the confidence intervals as a function of depth.

All time-resolved data sets were modeled by hand using refl1d, except for the data leading to the post-cycle 1 data, which evolved slowly enough to allow recursive fitting. The time resolved data shown in Fig 3br and Fig S23 were obtained by recursively fitting each R(Q) curve, also using the DREAM algorithm. The result of each fit was used as the initial model for the subsequent fit. The flat prior distribution used in the Bayesian approach of the DREAM algorithm mentioned above was replace by a Gaussian prior centered on the previous fit results, with a standard deviation of 3 Å for roughness parameters, 5 Å for thickness parameters, and $0.2 \times 10^{-6}/Å^2$ for SLD values.[2] These standard deviation values are significantly larger than the typical uncertainties on our fits to allow for substantial parameter changes as a function of time. The results were found to be stable under variations of those parameters, which mainly serve the purpose of avoiding unphysical solutions.

Binning of time-resolved neutron reflectivity data

For Figure 1, a binning time interval of 15 seconds was required because of the rapid changes observed at the electrode-electrolyte interface upon current application; no statistically significant change in the measured reflectivity curves was observed within a 15-sec interval when using finer intervals, and the bulk of the changes happen within the initial minute (Figure S7). Although time-resolved neutron reflectivity measurements were executed throughout the duration of application of j = -0.5 mA cm^{-2} (Figure S7), only measurements within the first minute could be satisfactorily modeled (Figure 1b, Table S3). This suggests that, by the conclusion of the first minute of chronopotentiometry, the material layers formed at the electrode-electrolyte interface became too thick, rough, and/or diffuse to obtain reflectivity profiles well-defined enough to model. This difficulty in modeling the reflectivity curves appears to correspond with the second decrease in potential following the observed potential plateau at t = 27 s (Figure 1a), which may suggest that this second decrease in potential is associated with the formation of much thicker, more diffuse layers at the electrode-electrolyte interface.

For Figure 3, a binning time interval of 30 seconds was used after employing the above analysis of the time-resolved reflectivity data for a variety of binning intervals. When modelling these time-resolved reflectivity curves, the thickness and SLD parameters of the Mo layer were held constant at the value of the final steady-state measurement (Table S1).

For Figure 4, as for the initial chronopotentiometry, we binned the reflectivity data into 15-sec increments. We were able to model reflectivity curves through t = 45 sec, after which the electrode-electrolyte interface became too rough and/or diffuse to model (Figure S24). The thickness and SLD of the Mo layer were again held constant during modeling of each of these reflectivity measurements.

Electrochemical Experiments at BL-4B

Electrochemical experiments were performed *in situ* during neutron reflectometry measurements using a Biologic VSP potentiostat in a three-electrode configuration.

Choice of Applied Current Density

The current density applied to the electrode was chosen based on the limitations associated with reflectometry measurements. In general, the maximum thickness of material that can be present on the electrode surface while still allowing for the measurement of reflectivity curves that can be satisfactorily modeled is 1000 – 2000 Å. For thicker layers, reflectivity fringe patterns become ill-defined and can no longer be modeled. Because we were interested in observing Li plating, we used the thickness of a plated Li layer as a rough estimate for a maximum current density that could be applied. Li plates according to the following equation:

$$Li^+(solution) + e^- \rightarrow Li(s)$$

Thus, the number of moles of Li that could be deposited to form a 2000-Å-thick layer of Li (density 0.534 g/cm^3 and molar mass 6.941 g/mol) on a surface was calculated as:

$$2000\ \text{Å}\ Li * \frac{cm}{1 \times 10^8\ \text{Å}} * \frac{0.534\ g}{cm^3} * \frac{mol}{6.941\ g} = 1.539 \times 10^{-6} \frac{mol\ Li}{cm^2}$$

This was converted to a current density for a time period of 2 min by:

$$1.539 \times 10^{-6} * \frac{1\ mol\ e^-}{1\ mol\ Li} * \frac{96485\ C}{mol\ e^-} * \frac{1}{120\ sec} = -1.2\ \frac{mA}{cm^2}$$

Thus, an estimate for the upper limit of a reasonable current density for a 2-min cycling period was determined to be ~ -1 mA/cm^2. However, because the thickness limitation can be as low as 1000 Å, we elected to halve this applied current density to -0.5 mA/cm^2 for this study in order to maximize our ability to measure interpretable reflectivity curves.

Benchtop Electrochemical Experiments

To evaluate the electrochemical performance toward Li-mediated N_2 reduction to NH_3, the electrochemical cell was prepared and filled with electrolyte as described above. The cell was then removed from the glovebox, and electrochemical experiments performed using a Biologic VMP-300 potentiostat in a three-electrode configuration. The electrolyte was then removed from the cell using a glass syringe and prepared for analysis via ^{1}HNMR by addition of 500 uL of electrolyte to an NMR tube followed by the sequential addition of 100 µL of 0.5 M H_2SO_4, 25 µL of d_6-DMSO (Fisher Scientific, 99.9%), and 50 µL EtOH (Sigma-Aldrich, 200 proof, anhydrous, ≥ 99.5%). A Varian Inova NMR spectrometer operating at 600 MHz was used to record sample spectra using a frequency-selective pulse sequence. Spectra were analyzed using MestreNova software.[3]

Sample Preparation for GI-XRD Experiments

50-nm thin films of Mo were deposited onto 35 x 5 mm Si wafer substrates using a custom electron-beam physical vapor deposition system (Technical Engineering Services) at a deposition rate of 0.1 Å /s. The Mo metal source target (99.95% purity, Kurt J. Lesker) was used as received. Prior to deposition, the Si wafer substrates (SEMI Standards, <100>, p-type, boron-doped, 0.1-0.9 Ω-cm) were sonicated for 30 minutes each in soapy water, 5:4:1 mixture of deionized water (18 MΩ cm): isopropanol: acetone, and finally deionized water only (18 MΩ cm).

Discussion of the lowering of the Mo thin film SLD

We considered factors that could produce a small lowering of the SLD of the Mo thin film. Such a lowering may be a result of changes in the microstructure of the Mo thin film over the course of chronopotentiometry. *In situ* GI-XRD (Figure S10) shows a broadening of the Mo peak (~2θ = 18.5°) during the application of a current density, which has been demonstrated to correlate with the appearance of dislocations and increased microstrain in Mo thin films.[4] We also investigated the effect of asymmetric surface roughness on fitted values. We estimate a systematic uncertainty of up to $\pm$ 0.2 10^{-6}/Å^2 on the Mo SLD value coming from different models leading to

similar fit quality. All models led to similar layer parameters for layers 1 and 2 and didn't change our conclusions.

Additional Discussion of GI-XRD Peaks in Figure 2

The appearance of the peak at $2\theta = 31.2^\circ$ across each of the conditions in Figure 2 might suggest that it could be related to solvent breakdown or an additional species such as LiSi that could be common across all experimental conditions. Solvent breakdown would be less likely, as the breakdown of THF typically forms amorphous species.[5–8] However, the lithiation of Si has been well-studied, and the peak at $2\theta = 31.2^\circ$ is near that of an expected LiSi peak (ICSD #78364), although the intensity is significantly greater than the intensity one would expect for this particular peak. We were additionally unable to attribute this peak to any of the following species: $LiClO_4$, LiN_5, Li_2C_2, Li_2C_{12}, Li_2CO_3, LiH, $LiMoN_2$, Li_4MoO_5, Li_2MoO_4, Li_4NH, $LiNH_2$, LiN_2, Li_2O_2, Li_2O, MoN, $MoSi_2$, Mo_3Si, or Si.

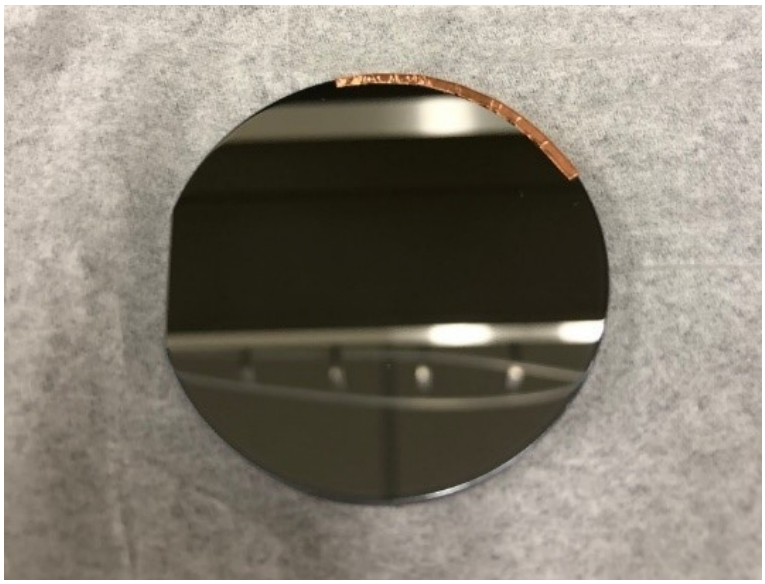

Figure S1. Photo of a representative cathode (50 nm of Mo on a Si wafer). Cu tape was placed on the edge of the Mo film to facilitate electrical contact between the film and the contact screw of the electrochemical cell. The tape was placed such that it was located outside of the chemically-resistant O-ring to avoid contact with the electrolyte.

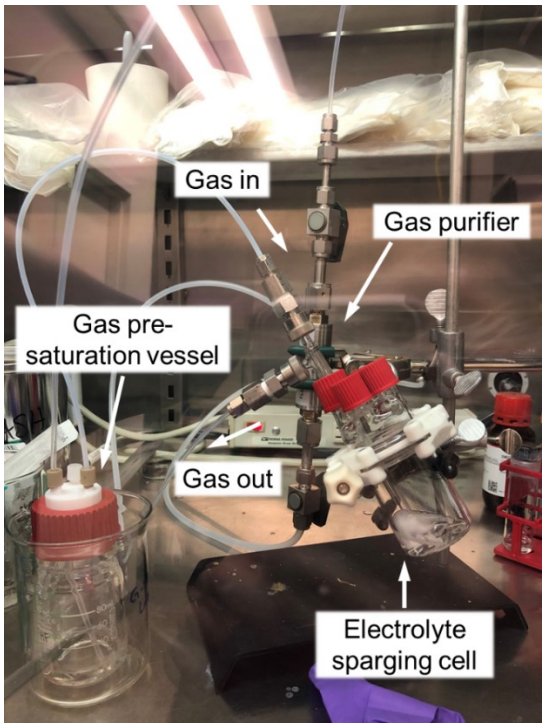

Figure S2. Electrolyte sparging in Ar glovebox. Inlet gas (N_2 or Ar) was flowed through a gas purifier into a pre-saturation vessel containing THF before flowing through a glass frit into a custom electrolyte sparging cell.

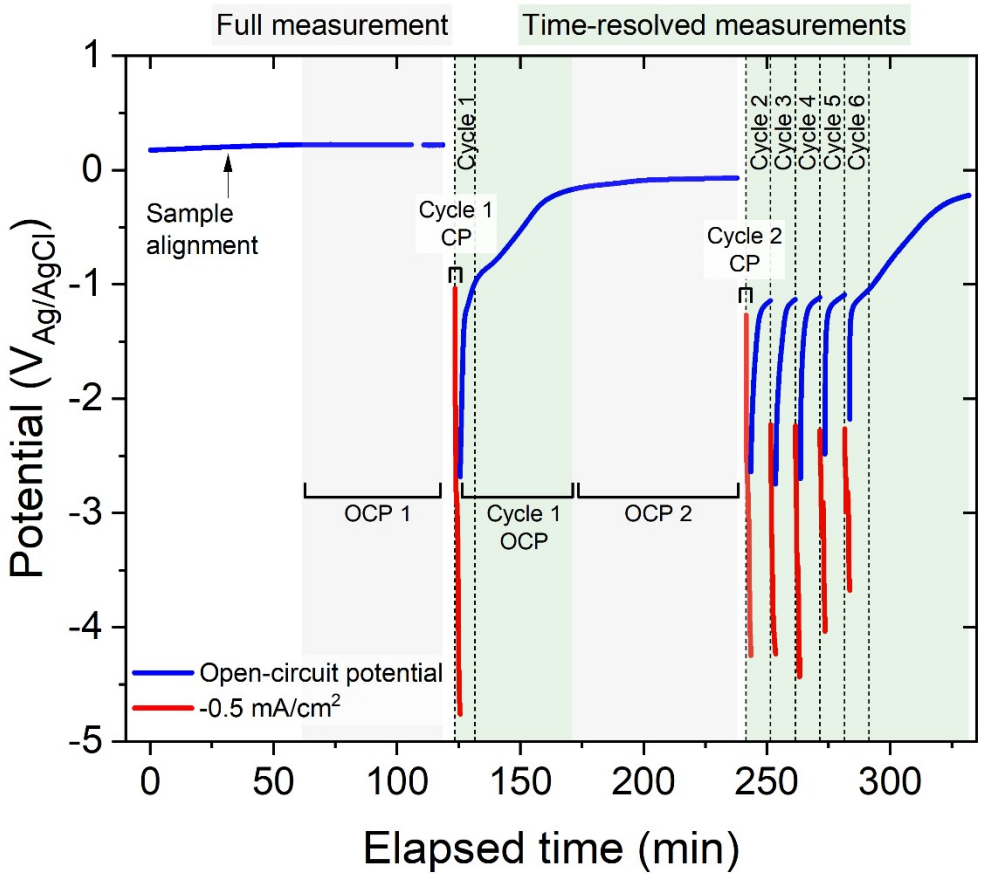

Figure S3. Potential versus time is shown for the electrochemical cell under electrochemical cycling conditions. Gray highlights indicate the time during which a "steady-state" neutron reflectivity measurement was taken, while green highlights correspond to times during the cycling experiment during which time-resolved neutron reflectivity measurements were taken. Blue curves correspond to the working electrode potential at open-circuit conditions, while red curves correspond to the working electrode potential during chronopotentiometry at a current density of -0.5 mA/cm^2. Sections of the plot are labeled with measurement names referred to in the main text: "OCP 1" is the steady-state neutron reflectivity measurement taken at OCP before a current density had been applied to the electrode, "Cycle 1 CP" is the time-resolved measurement taken during 2 min of application of -0.5 mA/cm^2 to the cathode, "Cycle 1 OCP" is the time-resolved measurement taken at OCP immediately following this application of -0.5 mA/cm^2 to the cathode, "OCP 2" is the steady-state measurement taken at OCP following this time-resolved measurement, and "Cycle 2 CP" is the time-resolved measurement taken during a second 2 min of application of -0.5 mA/cm^2 to the cathode during Cycle 2. The electrolyte was d_8-THF, 0.2 M $LiClO_4$, 0.17 M EtOH, sparged with purified N_2 for 15 minutes in an Ar glovebox.

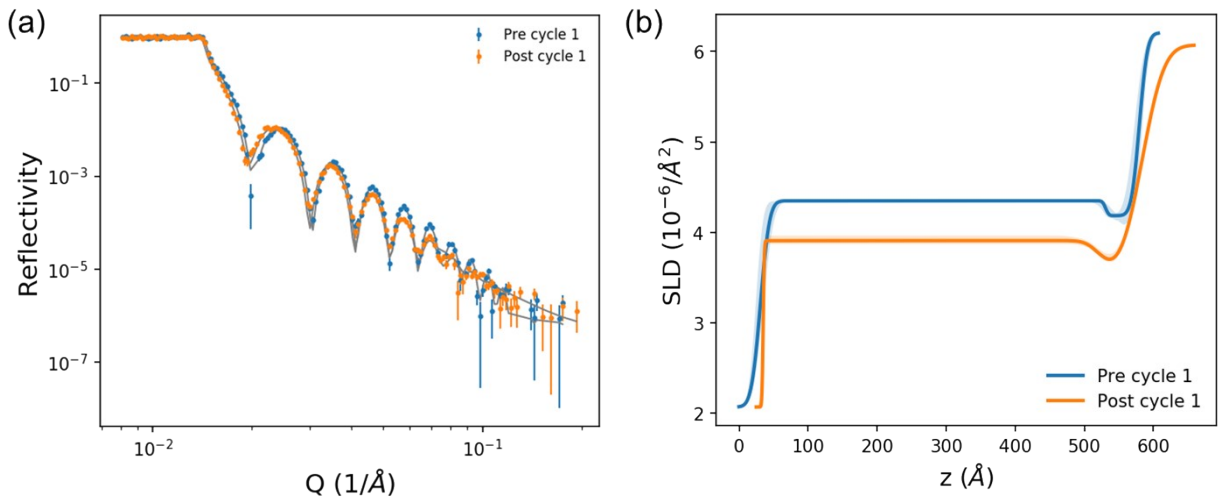

Figure S4. (a) Reflectivity curves of the electrode-electrolyte interface at open-circuit conditions in the electrochemical cell measured in the steady-state measurement configuration before (blue, OCP 1 in Figure S3) and after (orange, OCP 2 in Figure S3) the first cycle of chronopotentiometry at -0.5 mA/cm^2. Reflectivity data are shown as points, and corresponding models are shown as lines. The SLD profiles corresponding to these models are shown in (b). The electrolyte was d_8-THF, 0.2 M $LiClO_4$, 0.17 M EtOH, sparged with purified N_2 for 15 minutes in an Ar glovebox. Based on theoretical SLD calculations for pure MoO_2 and MoO_3, it might be expected that such an oxide layer would exhibit a larger SLD value than the modeled Mo layer (Table S2). However, such calculations assume a pure material phase and do not account for possible variations in density of a material layer. The observed surface layer in our model is thin and rough, which can be indicative of a low-density material, and our measurement is consistent with other studies that report oxide layers atop Mo as exhibiting lower SLD values than the Mo metal layer.[9]

Table S1. Model parameters corresponding to reflectivity curves presented in Figure S4. SLD values are provided in units of [10^{-6}/Å^2], thicknesses in units of [Å], and interfacial roughness in units of [Å].

TIME (SEC)	MO SLD	MO THICKNESS	MO INTERFACE	LAYER 1 SLD	LAYER 1 THICKNESS	LAYER 1 INTERFACE	THF SLD	THF INTERFACE	χ^2
PRE CYCLE 1	4.35 ± 0.01	500 ± 13	10.3 ± 1.1	4.19 ± 0.45	49 ± 14	3.7 ± 6.0	6.21 ± 0.01	9.1 ± 1.6	2.0
POST CYCLE 1	3.91 ± 0.03	489 ± 6	1.3 ± 0.6	3.55 ± 0.09	59.9 ± 6.8	16.8 ± 4.0	6.07 ± 0.02	24.9 ± 0.4	3.0

Table S2. Table of calculated SLD values for various species relevant to the NRR. Values were obtained using the Refl1d package via Oak Ridge National Laboratory.[10,11]

Layer	SLD (10^{-6}/Å^2)
MoO_2	5.581
MoO_3	4.735
Mo	4.308
$LiClO_4$	4.25
Li_2CO_3	3.485
Li_2O_2	2.368
Li_2C_2	1.962
Li_2O	0.812
Li_3N	0.804
LiOH	0.06
$LiNH_2$	-0.007
LiOEt	-0.143
Li	-0.88
LiH	-3.33

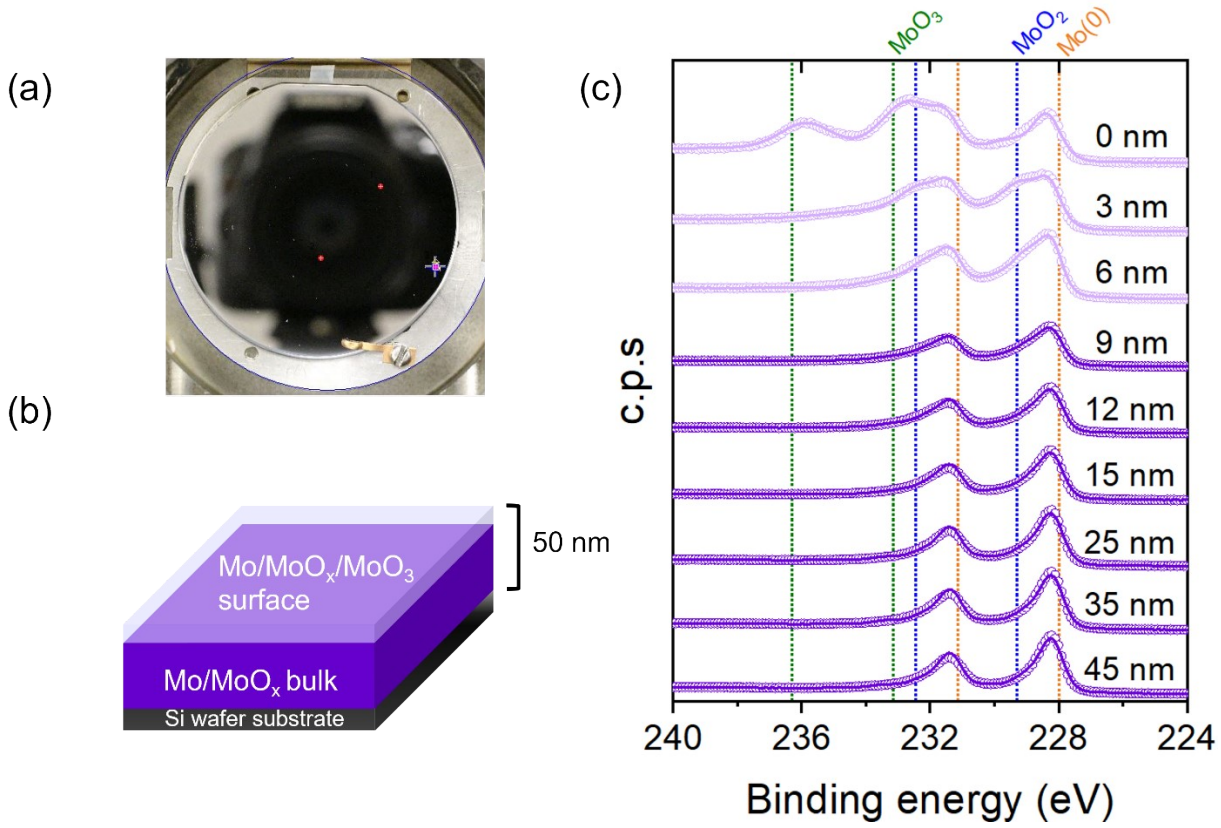

Figure S5. (a) Representative sample of 50 nm Mo deposited via PVD onto a 1-mm-thick, 2-inch-diameter Si wafer (SEMI Prime, p-type SI:B[111], Ro = 0.001-0.005 ohm-cm, El-Cat Inc.). A schematic of the cathode, shown in (b), was derived from the XPS depth profile of this sample that is shown in (c), where 0 nm corresponds to the surface of the sample, and 45 nm corresponds to the measurement taken after 45 nm of the sample surface were sputtered using an Ar gun at a sputtering rate of 3 nm/min. Drop lines corresponding to the locations of the Mo 3d doublets for Mo^0 (orange)[12], MoO_2 (blue),[13–15] and MoO_3 (green)[16] are shown.

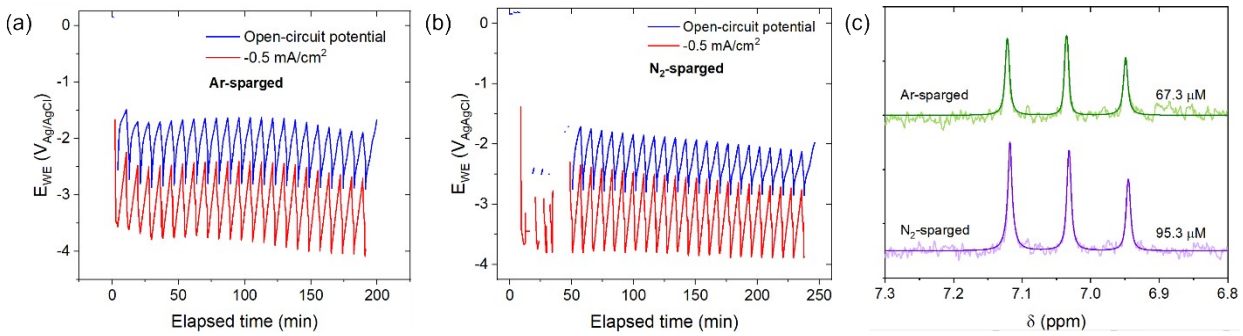

Figure S6. Benchtop electrochemical cycling experiments performed for NH_3 quantification in an electrolyte consisting of THF, 0.2 M $LiClO_4$, 0.17 M EtOH sparged with (a) purified Ar and (b) purified N_2. The electrolyte was prepared in an Ar glovebox and sparged using the apparatus shown in Figure S2. The electrochemical cell was filled in the glovebox, sealed, and removed from the glovebox for electrochemical testing to match electrochemical experiments performed at the neutron reflectometry beam line. The post-experiment electrolytes were then analyzed for NH_3 content via H^1NMR as shown in (c). The Ar-sparged NH_3 content corresponds to a Faradaic efficiency toward NH_3 of 0.07% while the N_2-sparged NH_3 content a Faradaic efficiency toward NH_3 of 0.09%.

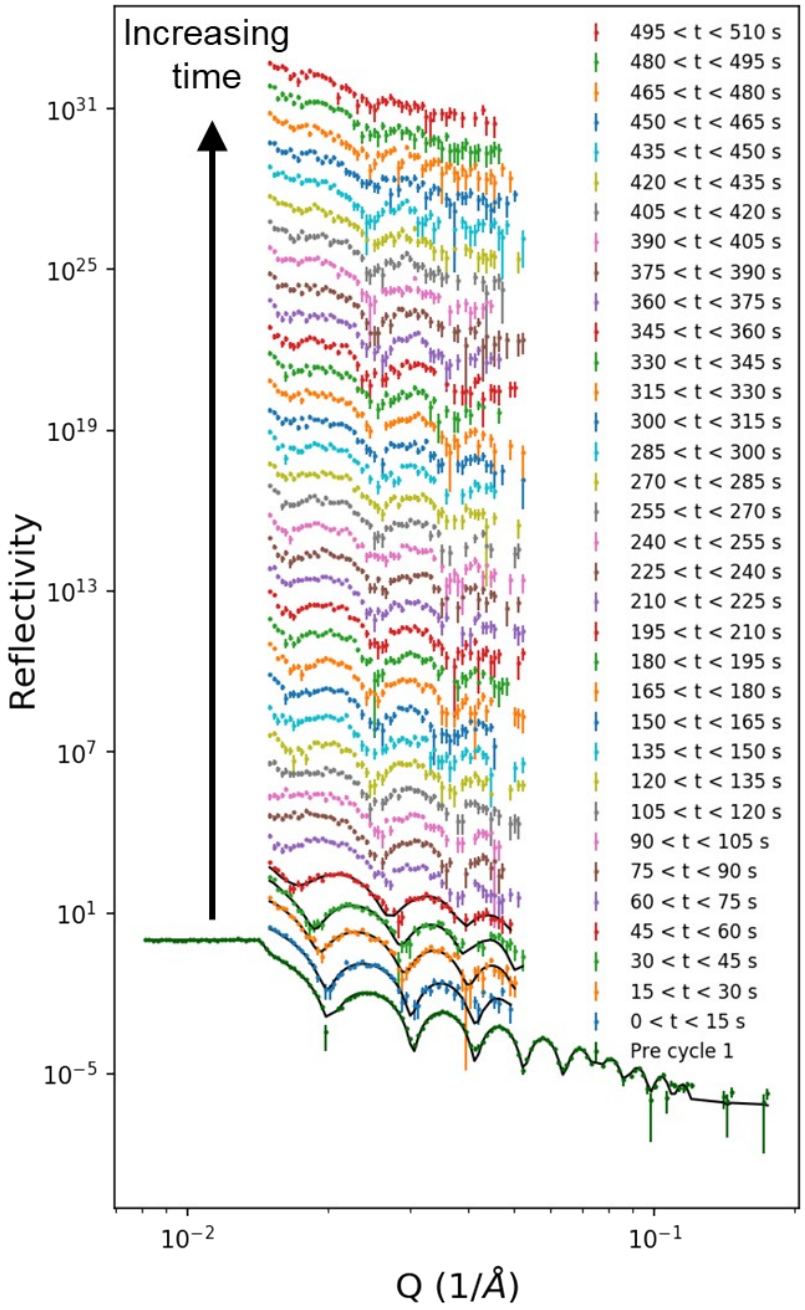

Figure S7. Time-resolved reflectivity measurements during chronopotentiometry at -0.5 mA/cm^2 for 2 min corresponding to Figure 1. Reflectivity data, shown as points, were binned into 15-sec increments to capture the dynamic changes observed at the electrode-electrolyte interface. Modeled reflectivity curves are shown as lines. The initial, steady-state measurement at open-circuit conditions is also shown in dark green at the bottom of the plot. Only the first four reflectivity curves were modeled; the remaining curves could not satisfactorily be fit but are shown to demonstrate the clear changes occurring at the electrode-electrolyte interface. The electrolyte consisted of d_8-THF, 0.2 M $LiClO_4$, 0.17 M EtOH pre-sparged with purified N_2.

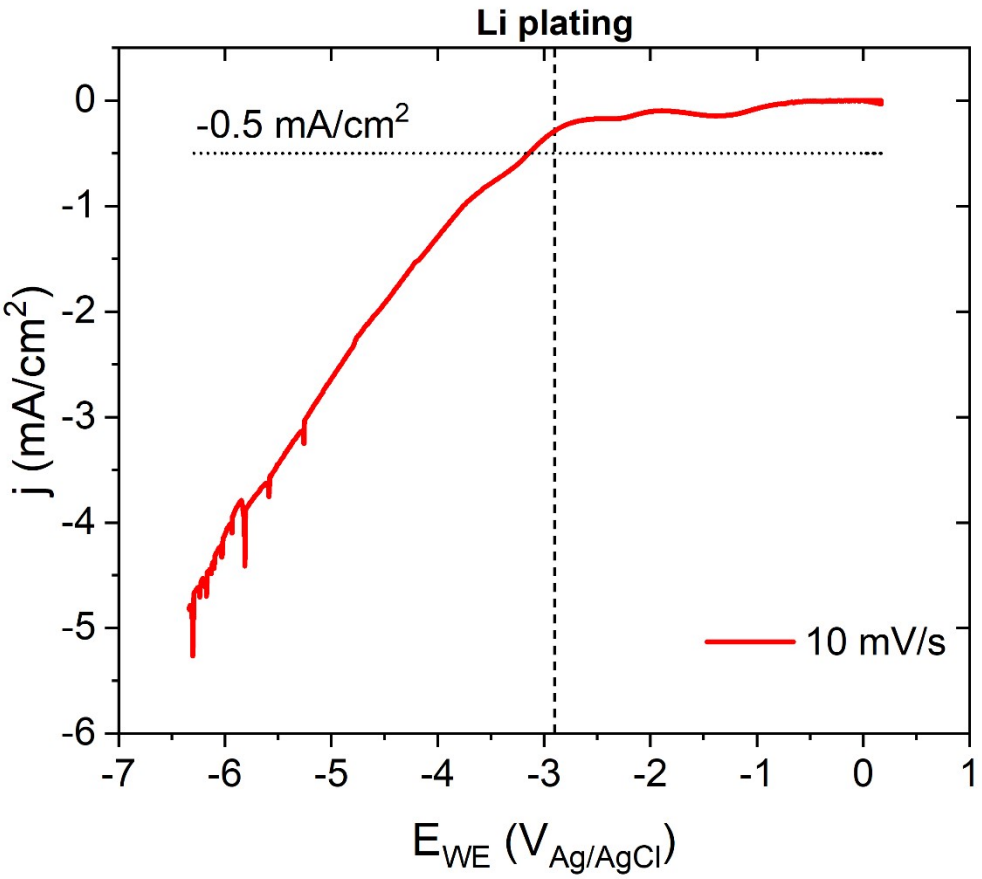

Figure S8. Linear-sweep voltammetry in the electrochemical cell to determine the likely onset of Li plating. The sweep was performed from 0 V to -6.5 V vs Ag/AgCl at a sweep rate of 10 mV/s. The approximate onset of Li plating as determined by the start of an increase in current density is marked with a dashed drop line, and a horizontal line corresponding to a current density of -0.5 mA/cm^2 is shown for reference. The electrolyte was d_8-THF, 0.2 M $LiClO_4$, 0.17 M EtOH, sparged with purified N_2 for 15 minutes in an Ar glovebox.

Table S3. Model parameters corresponding to fits shown in Figure 1 and Figure S8. These data correspond to the first period of constant current at -0.5 mA/cm^2. The quoted times correspond to the start of each time interval. SLD values are provided in units of [10^{-6}/Å^2], thicknesses in units of [Å], and interfacial roughness in units of [Å].

TIME (SEC)	MO SLD	MO THICKNESS	LAYER 1 SLD	LAYER 1 THICKNESS	LAYER 1 INTERFACE	LAYER 2 SLD	LAYER 2 THICKNESS	LAYER 2 INTERFACE	THF INTERFACE	χ^2
0<t<15	4.35 (fixed)	500 (fixed)	3.3 ± 0.6	46 ± 6	30 ± 7				16 ± 7	1.0
15<t<30	4.35 (fixed)	500 (fixed)	3.0 ± 0.2	63.9 ± 0.9	15 ± 2				17 ± 7	1.4
30<t<45	4.16 ± 0.05	516 ± 12	2.0 ± 1.2	48 ± 15	17 ± 4	5.9 ± 0.2	343 ± 51	25 ± 23	91 ± 15	1.5
45<t<60	4.12 ± 0.07	501 ± 2	-1.0 ± 0.6	244 ± 50	21 ± 3	5.3 ± 0.6	174 ± 38	83 ± 12	39 ± 21	1.1

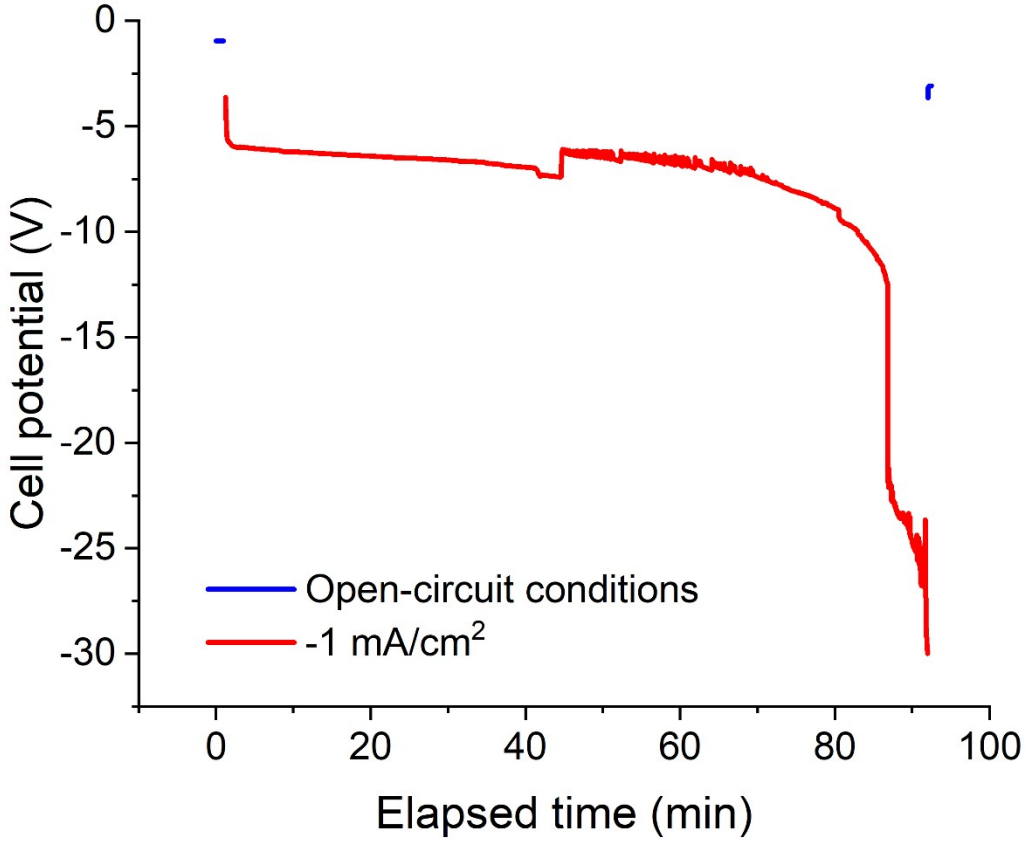

Figure S9. Chronopotentiometry at -1 mA/cm^2 in a custom *in situ* GI-XRD cell[17] carried out at BL 2-1 at the Stanford Synchrotron Radiation Lightsource (SSRL). The electrolyte was THF, 0.5 M $LiClO_4$, 0.17 M EtOH, sparged continuously with purified N_2 and pumped back and forth through the cell at a rate of 0.5 mL/min throughout the duration of the experiment. The cathode was 50 nm of Mo deposited onto a 35 mm x 5 mm Si wafer, while the anode was a Pt foil. Chronopotentiometry was carried out in a two-electrode configuration using a Biologic VSP potentiostat.

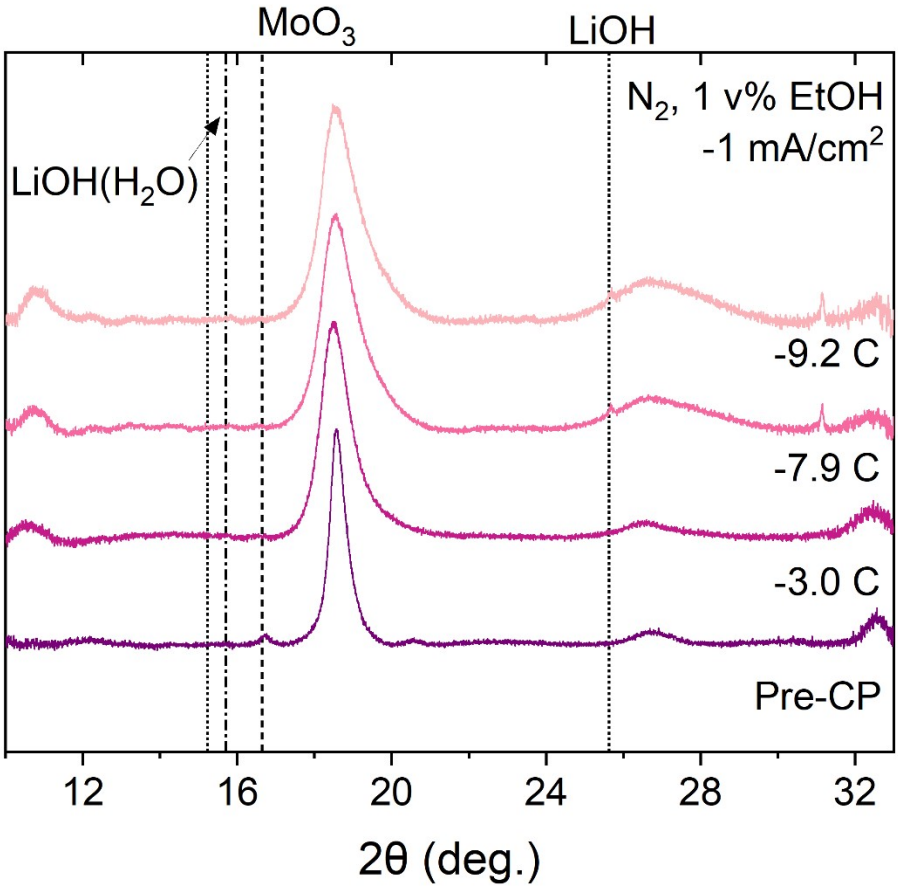

Figure S10. *In situ* GI-XRD diffractograms at various points of charge passed during chronopotentiometry at -1 mA/cm^2 shown in Figure S9. The electrolyte was THF, 0.5 M $LiClO_4$, 0.17 M EtOH, sparged continuously with purified N_2 and pumped back and forth through a custom *in situ* electrochemical cell[17] during GI-XRD measurements at 17 keV at BL 2-1 at the Stanford Synchrotron Radiation Lightsource (SSRL). Data were normalized to the Mo peak at 2θ = 18.6° after performing a manual background subtraction using a spline interpolation method. Drop lines show peak identities according to the ICSD reference patterns presented in Figure S12.

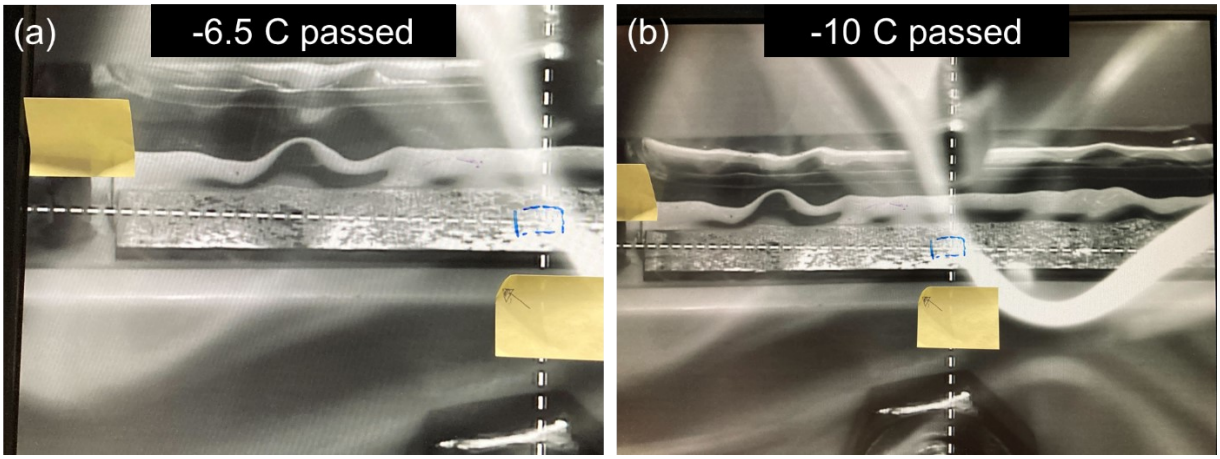

Figure S11. Photos of the cathode surface taken at two time points during the chronopotentiometry presented in Figure S9.

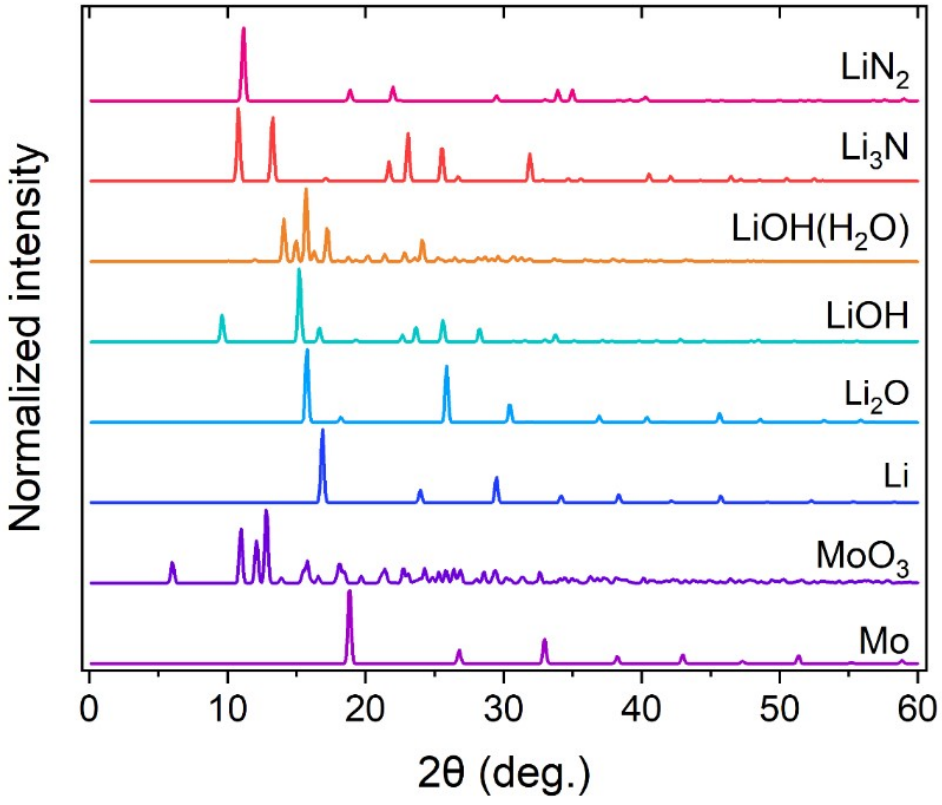

Figure S12. Reference XRD diffractograms taken from the ICSD database. The powder diffraction data were calculated using the ICSD interface for a wavelength of 0.729 Å, corresponding to the utilized X-ray energy of 17 keV at BL 2-1 at SSRL. The ICSD reference patterns are Mo (52267), MoO_3 (35076), Li (44367), Li_2O (54368), LiOH (26892), $LiOH(H_2O)$ (35155), Li_3N (34280), LiN_2 (25427).

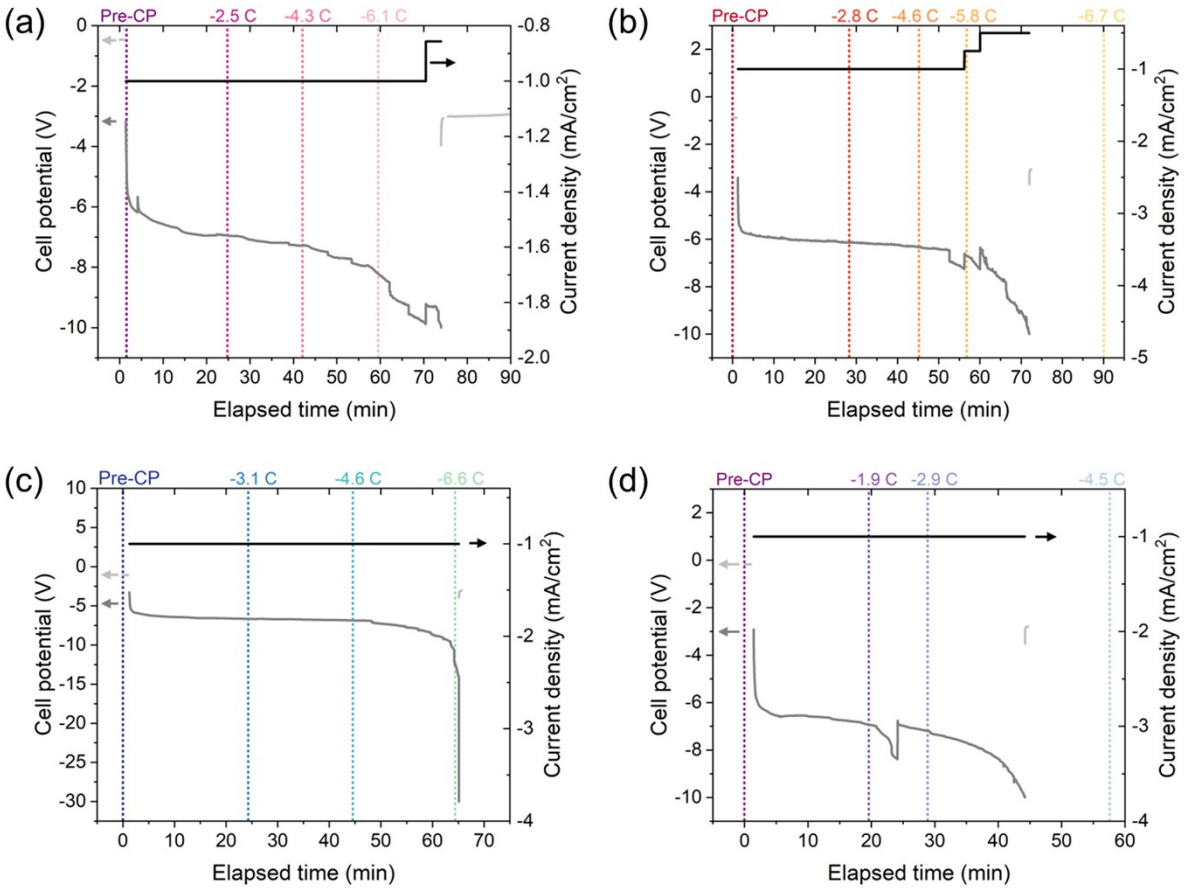

Figure S13. Chronopotentiometry at current densities of approximately -1 mA cm^{-2} in a two-electrode configuration corresponding to the GI-XRD measurements presented in Figure 2. The electrolyte conditions were THF with 0.5 M $LiClO_4$ and (a) no EtOH, sparged continuously with purified N_2, (b) 0.17 M EtOH, sparged continuously with purified N_2, (c) no EtOH, sparged continuously with purified Ar, and (d) 0.17 M EtOH, sparged continuously with purified Ar. The times at which the GI-XRD measurements were performed are indicated via droplines and are labeled with the charge passed at the time of measurement. Chronopotentiometry was continued until the potential reached the overload limit (10 V) of the potentiostat.

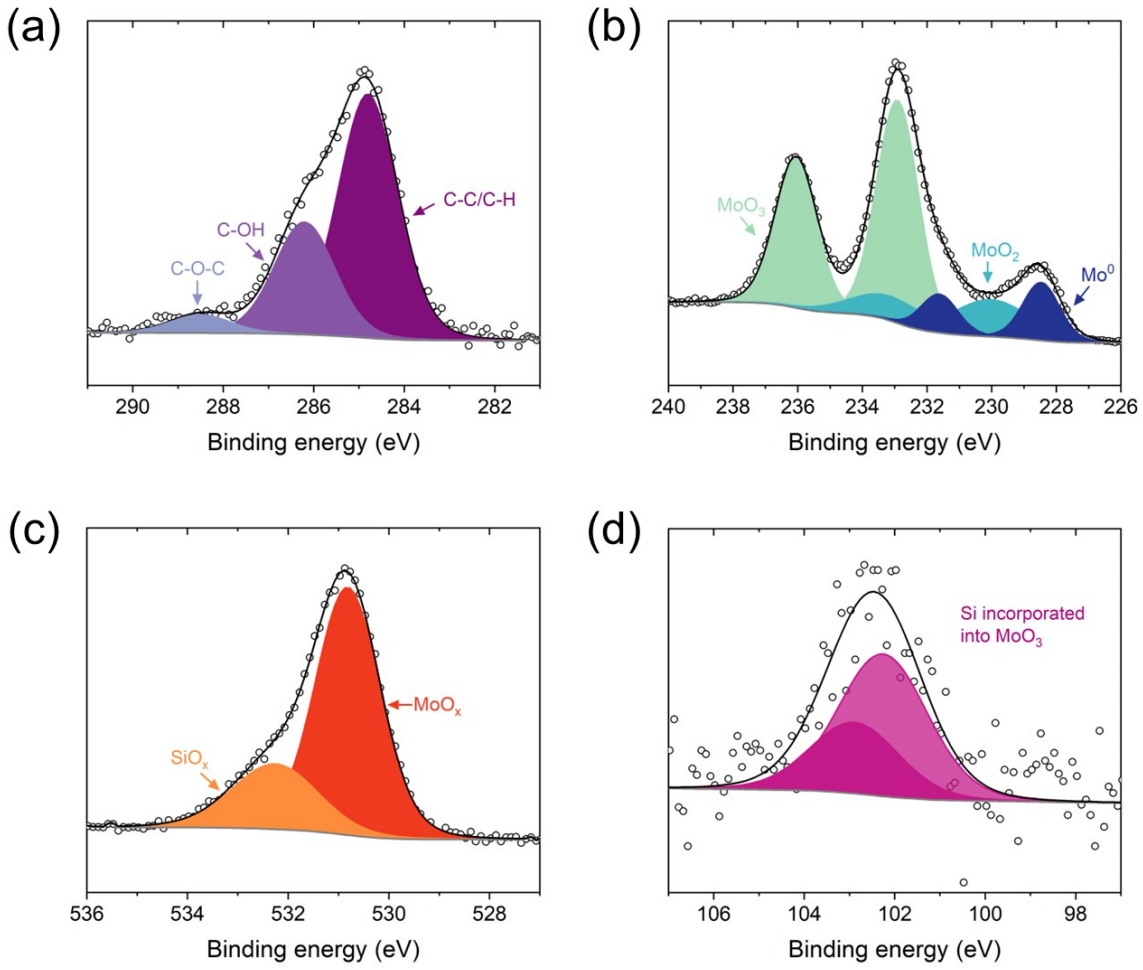

Figure S14. XPS of the surface of a representative working electrode (50 nm of Mo deposited via PVD onto a Si wafer) before chronopotentiometry. The C 1s spectrum is shown in (a), Mo 3d shown in (b), O 1s[18] shown in (c), and Si 2p[19] shown in (d).

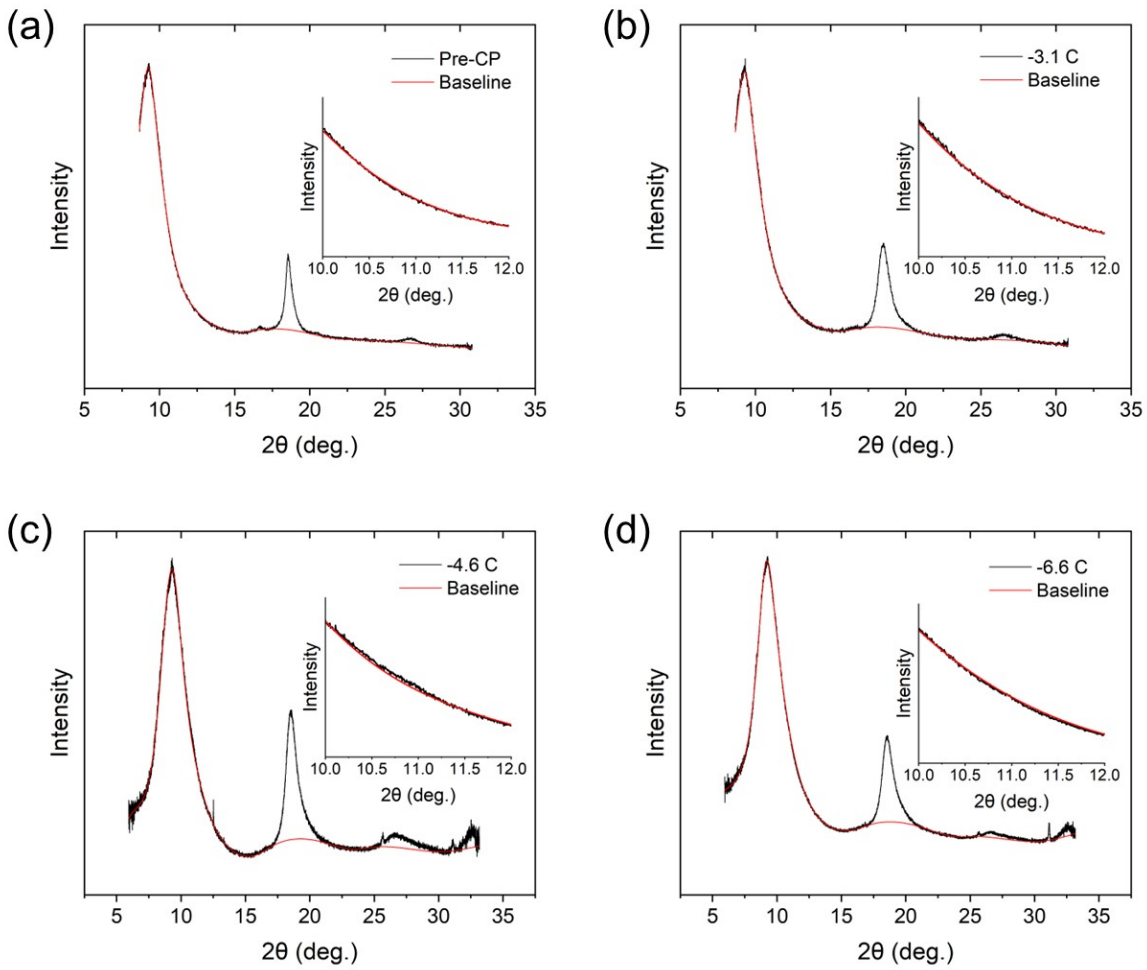

Figure S15. Raw data before background subtraction and normalization to the Mo peak at 18.5° for the GI-XRD measurements presented in Figure 2c, along with the baseline used for background subtraction of the GI-XRD data. Data for measurements taken after (a) 0 C, (b) -3.1 C, (c) -4.6 C, and (d) -6.6 C of charge passed are presented. Electrolyte conditions: 0.5 M $LiClO_4$ in THF, Ar-sparged, no EtOH.

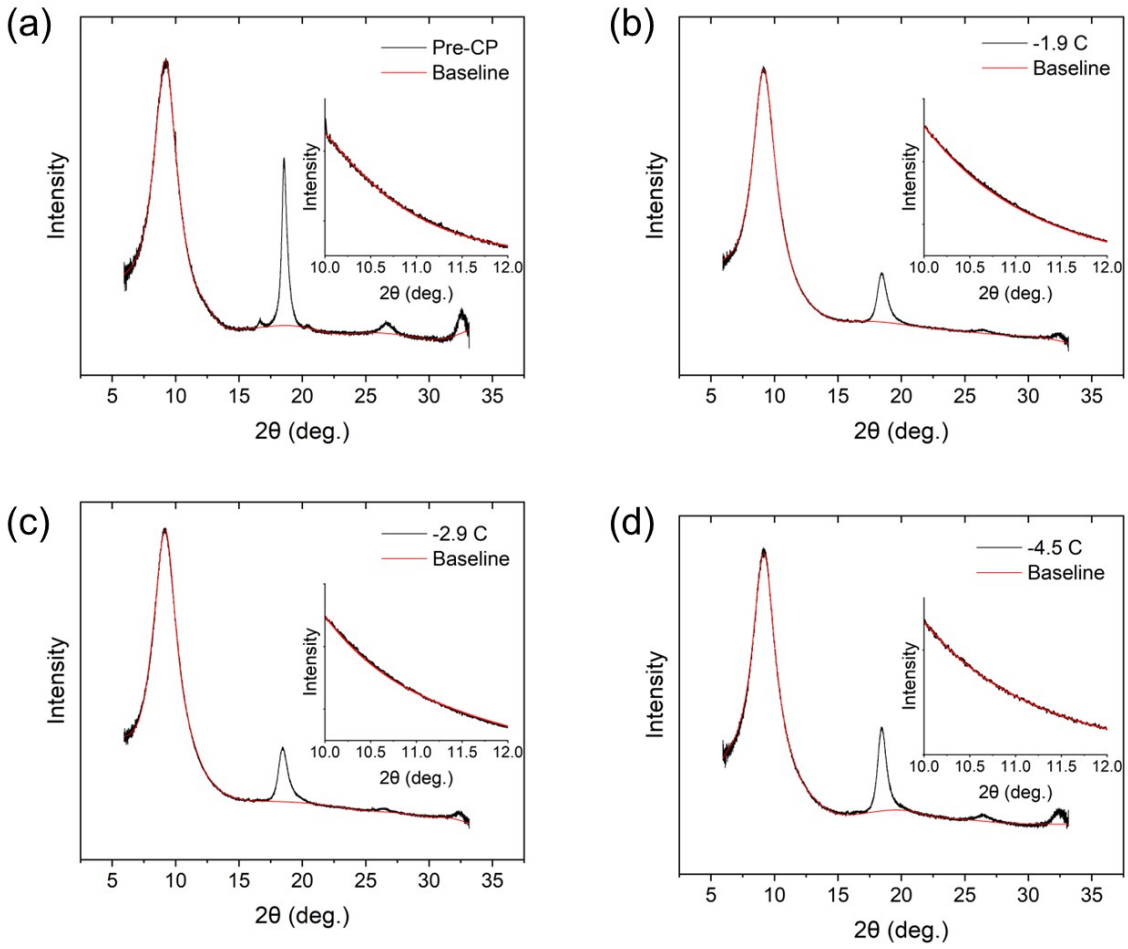

Figure S16. Raw data before background subtraction and normalization to the Mo peak at 18.5° for the GI-XRD measurements presented in Figure 2d, along with the baseline used for background subtraction of the GI-XRD data. Data for measurements taken after (a) 0 C, (b) -1.9 C, (c) -2.9 C, and (d) -4.5 C of charge passed are presented. Electrolyte conditions: 0.5 M $LiClO_4$ in THF, 0.17 M EtOH, Ar-sparged.

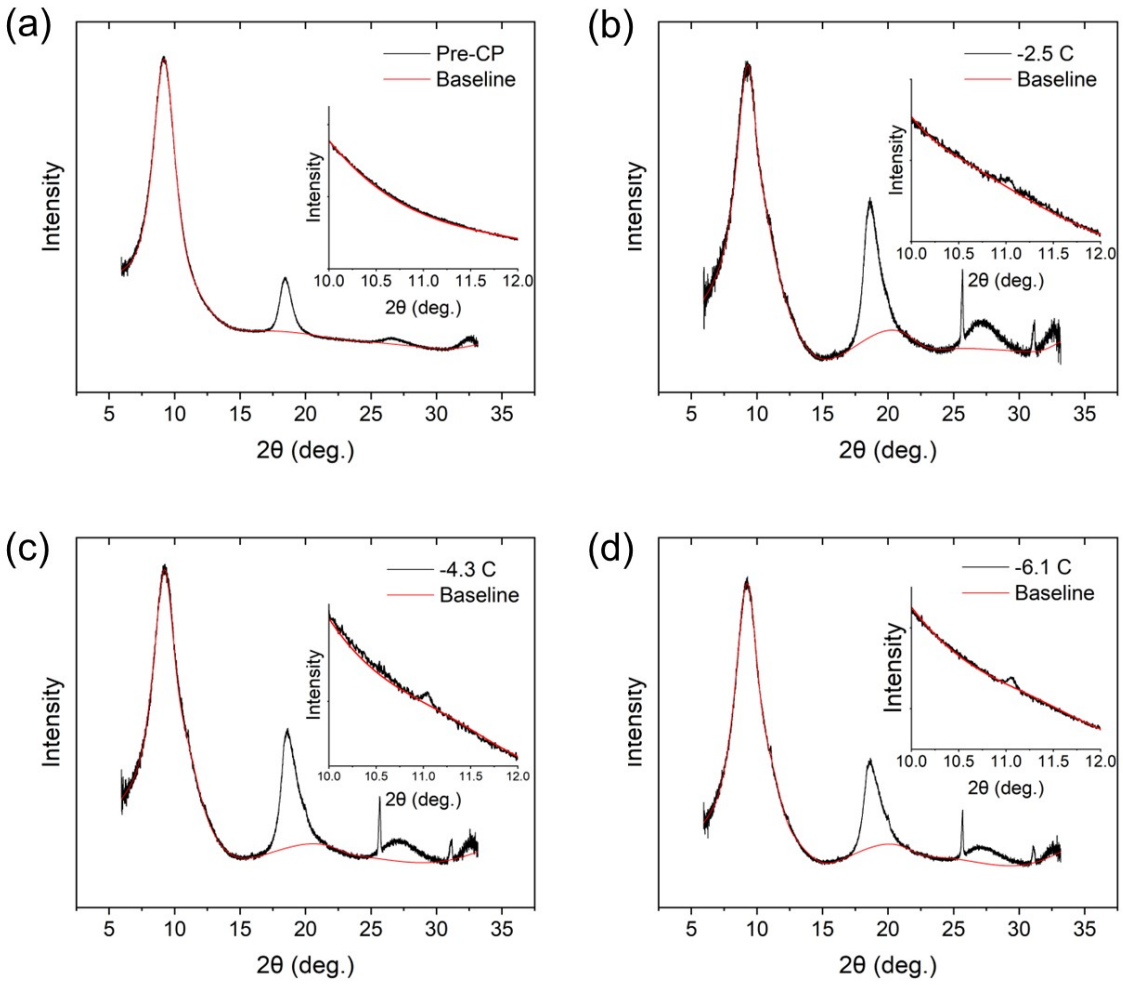

Figure S17. Raw data before background subtraction and normalization to the Mo peak at 18.5° for the GI-XRD measurements presented in Figure 2a, along with the baseline used for background subtraction of the GI-XRD data. Data for measurements taken after (a) 0 C, (b) -2.5 C, (c) -4.3 C, and (d) -6.1 C of charge passed are presented. Electrolyte conditions: 0.5 M $LiClO_4$ in THF, no EtOH, N_2-sparged.

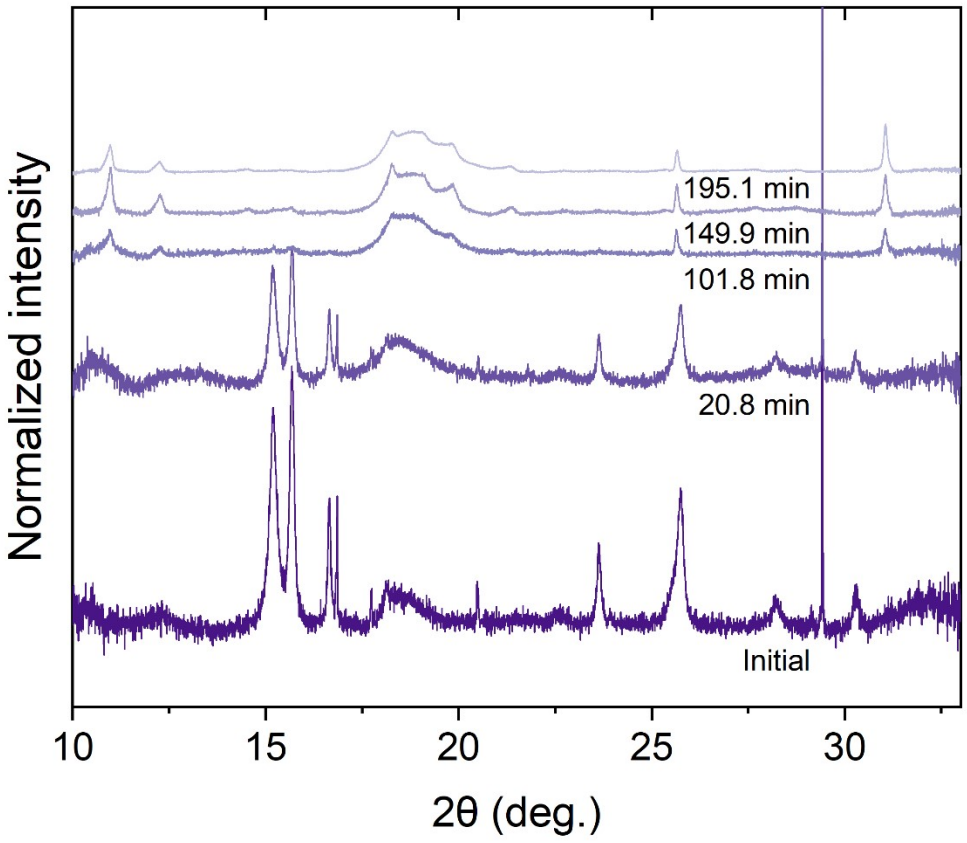

Figure S18. Synchrotron GI-XRD measurements of a piece of Li metal secured to the top of a sample (50 nm Mo on a Si wafer) at open-circuit conditions in the electrochemical cell over time. The electrolyte was THF, 0.5 M $LiClO_4$, no EtOH added. The electrolyte was sparged with purified Ar for the first GI-XRD measurement after which purified N_2 was sparged continuously into the electrolyte, which was being pumped back and forth through the cell at a rate of 0.3 mL/min.

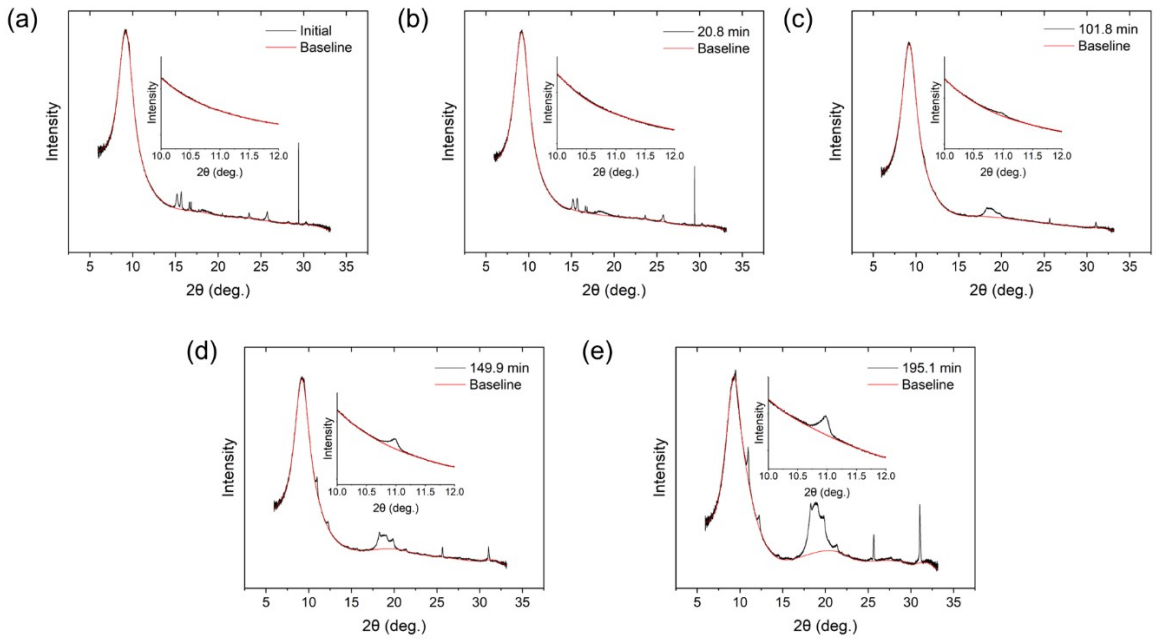

Figure S19. Raw data before background subtraction and normalization to the Mo peak at 18.5° for the GI-XRD measurements presented in Figure S18, along with the baseline used for background subtraction of the GI-XRD data. Data for measurements taken after (a) 0 min, (b) 20.8 min, (c) 101.8 min, (d) 149.9 min, and (e) 195.1 min of the Li foil sitting in the electrolyte at open-circuit conditions are presented.

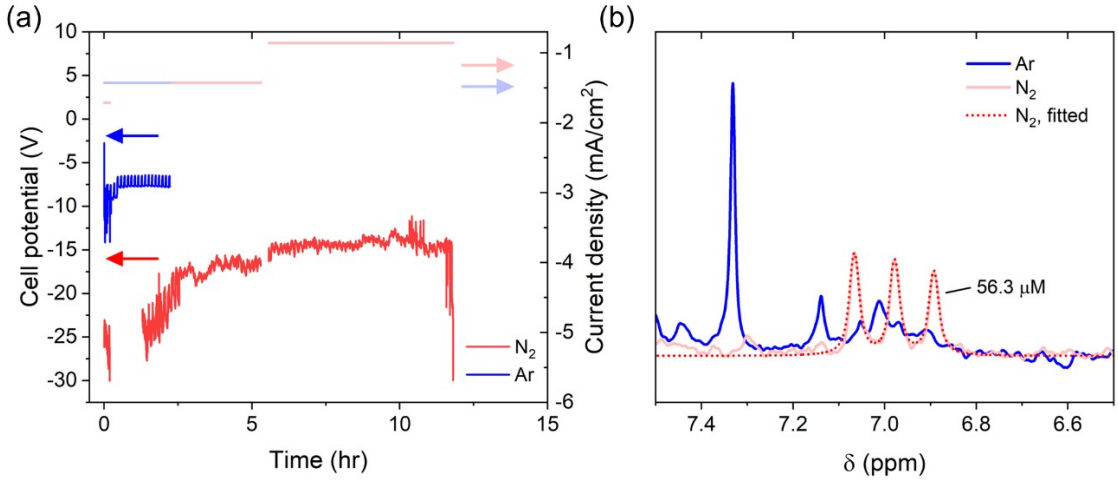

Figure S20. Chronopotentiometry performed in the GI-XRD cell in an Ar glovebox to confirm NH_3 production is shown in (a). The experiment was performed using a setup as close to the GI-XRD 'beam line' setup as possible: purified Ar (blue) or N_2 (red) were pre-saturated with THF, after which they were flowed directly into ~30 mL electrolyte in the electrolyte sparging vessel. This continuously-sparged electrolyte was pumped back and forth through the electrochemical cell during chronopotentiometry. The electrolyte was then collected from the electrolyte sparging vessel and analyzed for NH_3 content via H^1NMR (b). The electrolyte was THF, 0.5 M $LiClO_4$, 0.17 M EtOH.

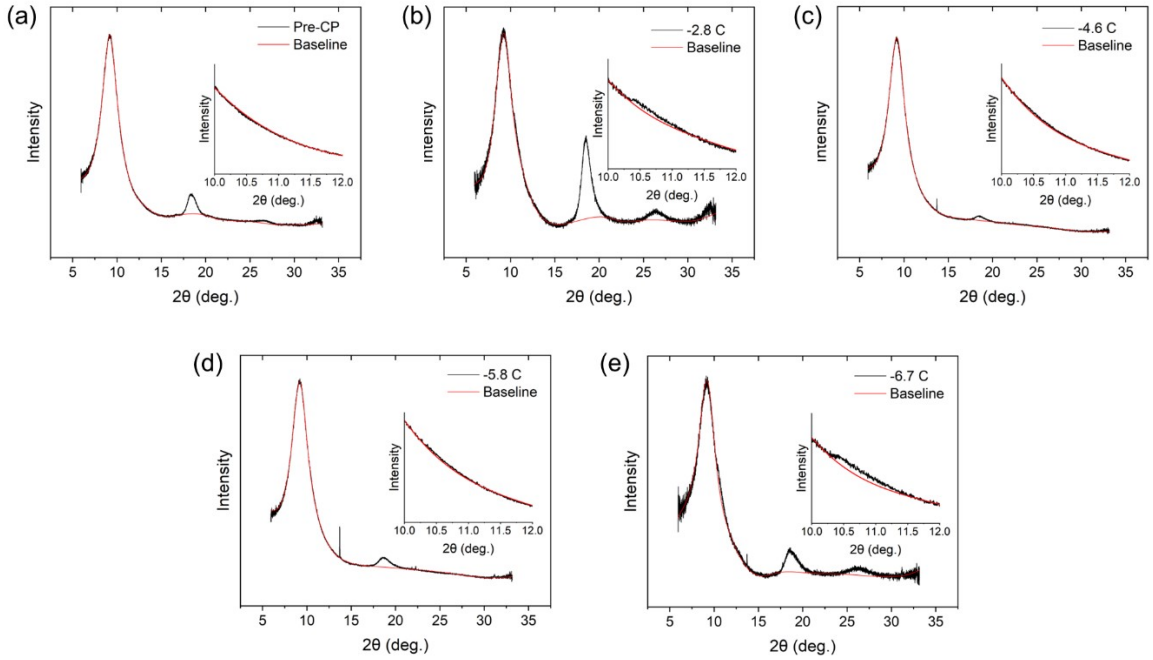

Figure S21. Raw data before background subtraction and normalization to the Mo peak at 18.5° for the GI-XRD measurements presented in Figure 2b, along with the baseline used for background subtraction of the GI-XRD data. Data for measurements taken after (a) 0 C, (b) -2.8 C, (c) -4.6 C, (d) -5.8 C, and (e) -6.7 C of charge passed are presented. Electrolyte conditions: 0.5 M $LiClO_4$ in THF, 0.17 M EtOH, N_2-sparged.

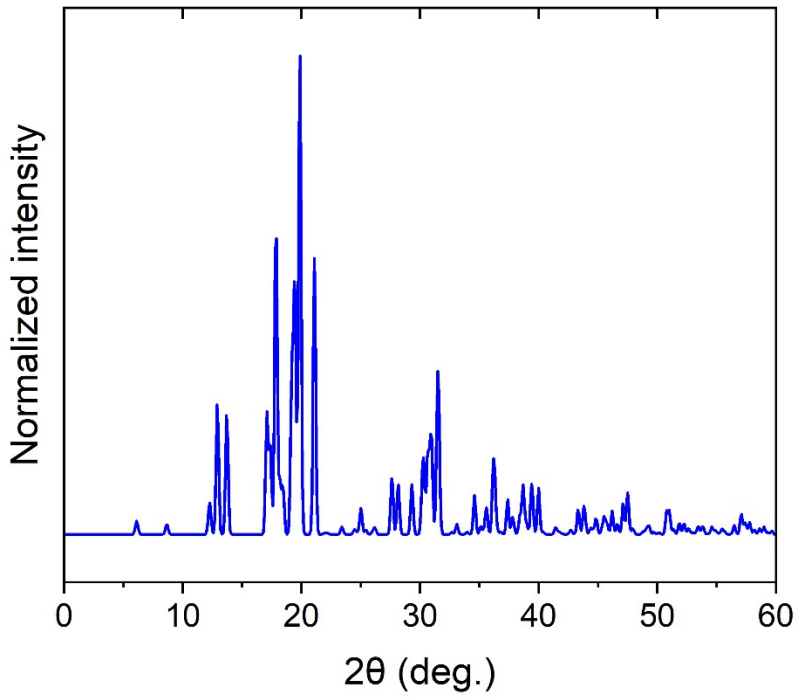

Figure S22. Reference XRD pattern of Mo_5Si_3 from the ICSD database (#143877) for an X-ray energy of 17 keV.

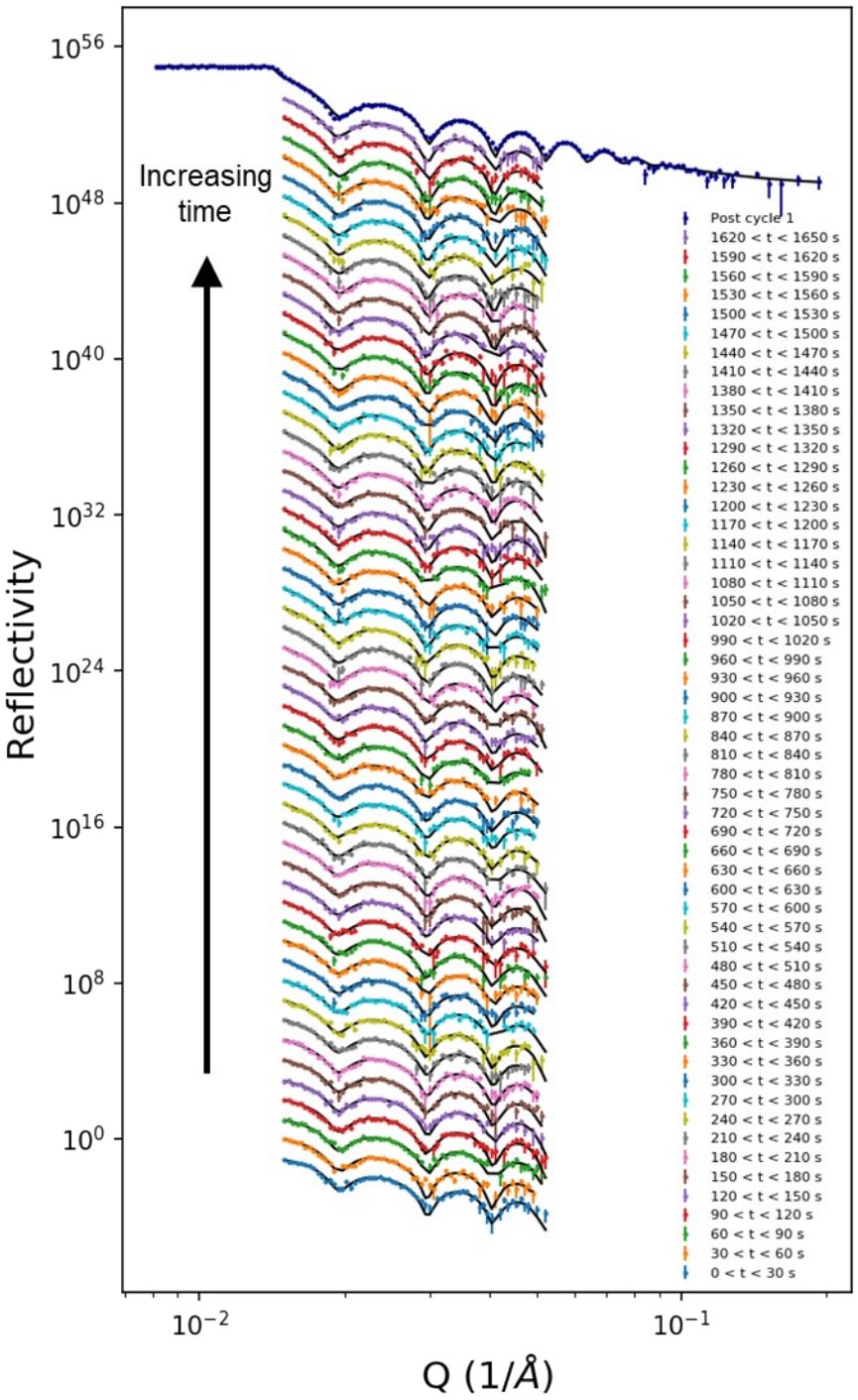

Figure S23. Time-resolved reflectivity data measured during the return of the electrochemical cell to open-circuit conditions shown in Figure 3 in the main text. Reflectivity data, binned into 30-sec increments, are shown as points, and modeled reflectivity curves are shown as lines. The initial, steady-state measurement at open-circuit conditions is also shown in dark blue. The electrolyte consisted of d_8-THF, 0.2 M $LiClO_4$, 0.17 M EtOH pre-sparged with purified N_2.

Table S4. Model parameters corresponding to the time-resolved reflectivity curve models presented in Figure S23. SLD values are provided in units of [10^{-6}/Å^2], thicknesses in units of [Å], and interfacial roughness in units of [Å]. Each timestamp corresponds to a 30-second binning interval (e.g. time t = 0 sec in the leftmost column corresponds to time interval $0 < t < 30$ sec).

TIME (SEC)	LAYER 1 SLD	LAYER 1 THICKNESS	LAYER 1 INTERFACE	LAYER 2 SLD	LAYER 2 THICKNESS	LAYER 2 INTERFACE	THF INTERFACE	χ^2
0	3.66 ± 0.07	66.5 ± 2.2	10.9 ± 2.4	5.72 ± 0.02	422.4 ± 6.0	11.5 ± 2.3	69.8 ± 4.7	1.07
30	3.78 ± 0.07	70.7 ± 2.4	11.8 ± 2.1	5.77 ± 0.02	417.2 ± 5.5	13.2 ± 2.7	71.5 ± 3.5	1.55
60	3.56 ± 0.07	65.4 ± 2.1	12.3 ± 2.2	5.74 ± 0.02	418.1 ± 5.2	12.4 ± 2.0	71.1 ± 3.3	0.91
90	3.60 ± 0.07	66.1 ± 2.1	12.1 ± 2.3	5.77 ± 0.02	415.1 ± 5.3	13.4 ± 2.3	72.3 ± 3.4	0.89
120	3.48 ± 0.07	63.8 ± 2.3	11.5 ± 2.5	5.74 ± 0.02	418.3 ± 5.2	14.0 ± 2.2	73.0 ± 3.4	1.25
150	3.51 ± 0.08	65.9 ± 2.2	11.4 ± 2.1	5.79 ± 0.02	417.3 ± 5.4	15.3 ± 2.7	73.5 ± 3.5	0.89
180	3.52 ± 0.08	65.7 ± 2.1	11.3 ± 2.2	5.82 ± 0.02	413.2 ± 5.4	16.2 ± 2.8	73.0 ± 3.4	1.12
210	3.48 ± 0.09	66.8 ± 2.2	11.7 ± 2.2	5.83 ± 0.02	412.7 ± 5.3	17.4 ± 2.7	73.9 ± 3.3	1.29
240	3.50 ± 0.08	68.2 ± 2.1	10.9 ± 2.3	5.83 ± 0.02	410.9 ± 5.3	17.4 ± 2.8	74.2 ± 3.4	1.34
270	3.37 ± 0.09	64.3 ± 2.2	11.6 ± 2.2	5.84 ± 0.02	411.9 ± 5.5	16.4 ± 2.6	74.3 ± 3.4	1.08
300	3.40 ± 0.09	65.1 ± 2.2	11.3 ± 2.2	5.85 ± 0.02	411.4 ± 5.4	17.9 ± 2.7	74.9 ± 3.4	1.48
330	3.38 ± 0.09	64.9 ± 2.1	11.8 ± 2.2	5.86 ± 0.02	410.2 ± 5.4	17.4 ± 2.6	74.9 ± 3.3	1.13
360	3.43 ± 0.09	66.7 ± 2.0	13.0 ± 2.5	5.85 ± 0.02	407.5 ± 5.4	18.3 ± 2.9	75.6 ± 3.4	1.32
390	3.38 ± 0.09	65.0 ± 2.1	13.9 ± 2.6	5.86 ± 0.02	405.3 ± 5.3	19.0 ± 2.6	76.1 ± 3.4	1.41
420	3.29 ± 0.09	65.1 ± 2.1	15.1 ± 2.7	5.86 ± 0.02	403.8 ± 5.3	19.4 ± 2.6	77.0 ± 3.3	1.2
450	3.28 ± 0.09	64.2 ± 2.1	14.9 ± 2.8	5.87 ± 0.02	404.6 ± 5.6	18.9 ± 2.5	78.2 ± 3.3	1.04
480	3.24 ± 0.10	62.9 ± 2.1	14.2 ± 2.8	5.87 ± 0.02	404.4 ± 5.4	18.2 ± 2.7	78.2 ± 3.3	0.9
510	3.31 ± 0.09	63.9 ± 2.1	13.2 ± 2.5	5.87 ± 0.02	403.3 ± 5.4	17.9 ± 2.7	79.0 ± 3.3	1.1
540	3.36 ± 0.09	65.2 ± 2.1	13.2 ± 2.4	5.87 ± 0.02	401.5 ± 5.4	18.9 ± 2.7	80.2 ± 3.3	1.15
570	3.31 ± 0.09	64.3 ± 2.1	12.4 ± 2.3	5.90 ± 0.02	398.4 ± 5.4	16.8 ± 2.6	81.3 ± 3.3	1.09
600	3.29 ± 0.10	64.6 ± 2.2	13.5 ± 2.6	5.89 ± 0.02	397.8 ± 5.4	22.6 ± 2.5	80.2 ± 3.4	1.21
630	3.24 ± 0.10	64.8 ± 2.2	14.2 ± 2.7	5.89 ± 0.02	400.1 ± 5.3	21.2 ± 2.5	80.5 ± 3.4	1.17
660	3.25 ± 0.10	63.1 ± 2.2	13.2 ± 2.6	5.87 ± 0.02	399.8 ± 5.4	20.7 ± 2.5	81.6 ± 3.4	1.19
690	3.22 ± 0.10	62.3 ± 2.2	13.0 ± 2.4	5.89 ± 0.02	397.7 ± 5.3	20.6 ± 2.6	82.1 ± 3.2	1.32
720	3.29 ± 0.10	65.1 ± 2.2	13.4 ± 2.7	5.88 ± 0.02	395.9 ± 5.3	22.2 ± 2.5	81.3 ± 3.4	1.3
750	3.28 ± 0.10	64.0 ± 2.4	11.6 ± 2.4	5.88 ± 0.02	393.0 ± 5.4	21.6 ± 2.7	81.5 ± 3.3	1.05
780	3.22 ± 0.11	61.6 ± 2.3	11.2 ± 2.4	5.87 ± 0.02	388.3 ± 5.3	23.8 ± 2.5	81.2 ± 3.3	0.97
810	3.36 ± 0.11	63.8 ± 2.5	10.6 ± 2.0	5.90 ± 0.02	385.1 ± 5.5	21.8 ± 2.9	80.1 ± 3.4	1.41
840	3.36 ± 0.10	64.2 ± 2.4	10.4 ± 2.1	5.90 ± 0.02	385.3 ± 5.6	22.1 ± 2.5	79.8 ± 3.3	1.12
870	3.37 ± 0.10	64.5 ± 2.4	10.2 ± 2.0	5.89 ± 0.02	384.6 ± 5.6	22.0 ± 2.6	79.7 ± 3.4	1.05
900	3.41 ± 0.10	64.5 ± 2.3	10.2 ± 1.8	5.92 ± 0.02	384.4 ± 5.7	22.0 ± 2.6	79.7 ± 3.3	1.13
930	3.37 ± 0.10	63.8 ± 2.1	10.6 ± 1.9	5.94 ± 0.02	384.1 ± 5.5	22.0 ± 2.6	80.2 ± 3.2	1.13
960	3.36 ± 0.10	64.4 ± 2.4	10.8 ± 2.0	5.88 ± 0.02	380.4 ± 5.3	22.8 ± 2.6	80.8 ± 3.4	1.3
990	3.35 ± 0.10	64.2 ± 2.3	10.9 ± 2.0	5.93 ± 0.02	380.2 ± 5.4	22.5 ± 2.7	80.9 ± 3.4	1.12
1020	3.41 ± 0.11	65.3 ± 2.4	10.8 ± 2.1	5.92 ± 0.02	377.9 ± 5.6	23.7 ± 2.7	80.8 ± 3.5	1.12
1050	3.45 ± 0.11	65.4 ± 2.5	10.8 ± 2.1	5.96 ± 0.02	377.4 ± 5.6	23.8 ± 2.6	81.3 ± 3.4	0.9

1080	3.41 ± 0.10	64.2 ± 2.4	11.3 ± 2.0	5.92 ± 0.02	372.7 ± 5.7	22.5 ± 2.7	81.6 ± 3.5	1.27
1110	3.39 ± 0.10	63.6 ± 2.3	12.4 ± 2.1	5.91 ± 0.02	370.2 ± 5.5	22.4 ± 2.6	81.7 ± 3.4	1.09
1140	3.43 ± 0.10	65.3 ± 2.4	12.3 ± 2.3	5.93 ± 0.02	369.7 ± 5.4	23.6 ± 2.6	81.4 ± 3.4	1.01
1170	3.41 ± 0.10	65.3 ± 2.5	12.5 ± 2.5	5.93 ± 0.02	369.6 ± 5.5	23.6 ± 2.6	81.5 ± 3.4	1.44
1200	3.44 ± 0.10	64.0 ± 2.4	12.7 ± 2.5	5.93 ± 0.02	370.9 ± 5.6	23.6 ± 2.5	81.6 ± 3.3	1.12
1230	3.45 ± 0.11	63.4 ± 2.5	13.0 ± 2.4	5.96 ± 0.02	369.2 ± 5.5	23.5 ± 2.7	81.2 ± 3.3	1.11
1260	3.28 ± 0.11	61.7 ± 2.4	13.6 ± 2.6	5.93 ± 0.02	366.0 ± 5.5	25.5 ± 2.3	81.8 ± 3.3	1.3
1290	3.33 ± 0.12	61.5 ± 2.6	13.7 ± 2.7	5.96 ± 0.02	365.4 ± 5.5	25.5 ± 2.4	81.5 ± 3.3	1.19
1320	3.27 ± 0.13	63.6 ± 2.8	12.8 ± 2.4	5.96 ± 0.02	363.6 ± 5.8	29.6 ± 2.6	82.0 ± 3.3	1.18
1350	3.21 ± 0.13	59.1 ± 2.6	11.6 ± 2.3	5.95 ± 0.02	362.0 ± 5.6	28.9 ± 2.5	82.4 ± 3.3	0.91
1380	3.16 ± 0.13	55.5 ± 2.5	11.7 ± 2.2	5.93 ± 0.02	359.6 ± 5.5	26.6 ± 2.2	82.0 ± 3.3	1.29
1410	3.19 ± 0.12	59.8 ± 2.7	12.1 ± 2.3	5.96 ± 0.02	356.9 ± 5.5	30.9 ± 1.9	81.5 ± 3.4	1.02
1440	3.16 ± 0.14	57.7 ± 2.8	11.8 ± 2.2	5.98 ± 0.02	354.5 ± 5.6	32.2 ± 2.2	81.0 ± 3.4	1.55
1470	3.09 ± 0.13	56.5 ± 2.7	12.0 ± 2.2	5.98 ± 0.02	351.9 ± 5.6	33.0 ± 1.6	80.8 ± 3.3	1.18
1500	2.99 ± 0.13	55.1 ± 2.6	12.0 ± 2.1	5.98 ± 0.02	349.4 ± 5.6	32.6 ± 1.5	80.2 ± 3.3	0.88
1530	2.97 ± 0.12	55.0 ± 2.6	11.9 ± 2.3	5.99 ± 0.02	348.7 ± 5.5	32.5 ± 1.3	80.1 ± 3.4	1.47
1560	3.20 ± 0.11	58.2 ± 2.6	11.7 ± 2.2	5.99 ± 0.02	345.4 ± 5.6	32.5 ± 1.1	79.5 ± 3.5	1.13
1590	3.20 ± 0.13	57.8 ± 2.7	11.5 ± 1.9	6.01 ± 0.02	344.6 ± 5.6	32.5 ± 1.6	78.5 ± 3.4	1.06
1620	3.11 ± 0.12	58.4 ± 2.6	11.6 ± 2.1	6.00 ± 0.02	344.5 ± 5.7	33.1 ± 1.5	78.5 ± 3.4	1.12
1650	3.21 ± 0.15	58.3 ± 3.7	10.7 ± 2.2	6.00 ± 0.03	345.6 ± 5.7	34.1 ± 1.5	78.2 ± 3.4	1.17

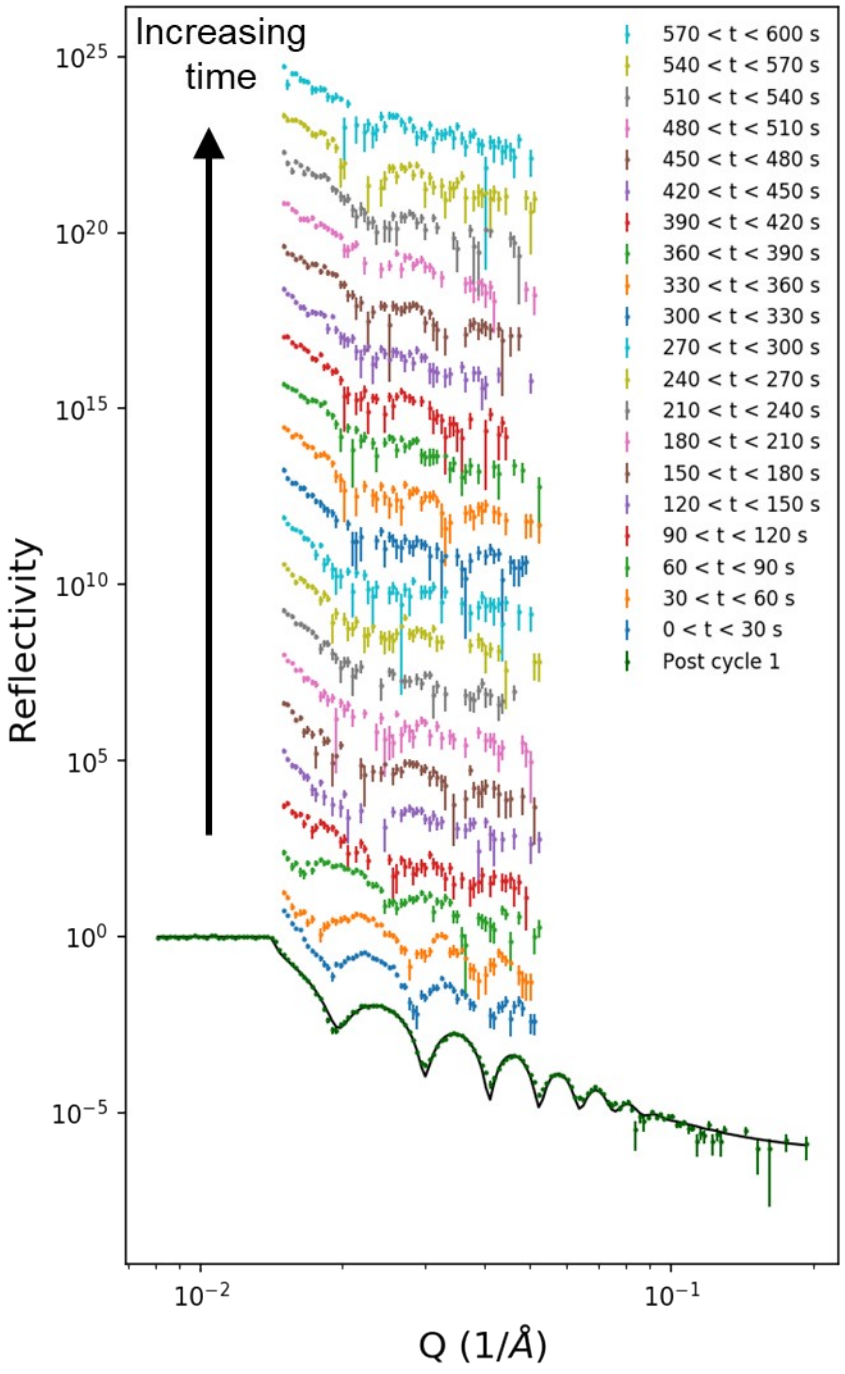

Figure S24. Time-resolved reflectivity measurements during the second-cycle chronopotentiometry at -0.5 mA/cm^2 for 2 min corresponding to Figure 4. Reflectivity data, shown as points, were binned into 30-sec increments for this figure. The steady-state measurement at open-circuit conditions (OCP 2), along with the modeled reflectivity curve, is also shown in dark green. The electrolyte consisted of d_8-THF, 0.2 M $LiClO_4$, 0.17 M EtOH pre-sparged with purified N_2.

Table S5. Model parameters corresponding to reflectivity curves shown in Figure 4 in the main text. SLD values are provided in units of [10^{-6}/Å^2], thicknesses in units of [Å], and interfacial roughness in units of [Å].

TIME (SEC)	LAYER 1 SLD	LAYER 1 THICKNESS	LAYER 1 INTERFACE	LAYER 2 SLD	LAYER 2 THICKNESS	LAYER 2 INTERFACE	THF INTERFACE	χ^2
0 < t < 15	3.17 ± 0.17	77.2 ± 4.3	15.0 ± 7.1				40.0 ± 4.1	1.3
15 < t < 30	3.06 ± 0.26	112.1 ± 5.4	5 ± 10	5.85 ± 0.42	216 ± 73	40 ± 11	28 ± 33	1.3
30 < t < 45	2.66 ± 0.27	96.0 ± 8.7	22 ± 10	3.71 ± 0.46	359 ± 80	10.1 ± 4.2	148 ± 13	1.5

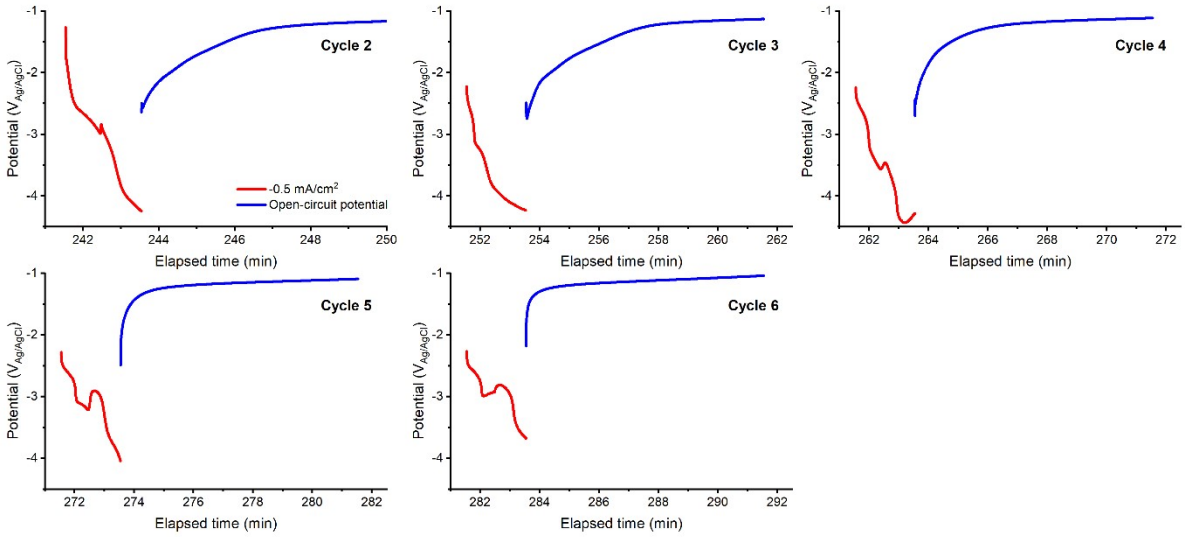

Figure S25. Chronopotentiometry at -0.5 mA/cm^2 for Cycles 2-6 in the electrochemical cell. Reflectivity curves for Cycles 3-6 could not be fit to a model to a satisfactory level.

References

(1) Vrugt, J. A.; ter Braak, C. J. F.; Diks, C. G. H.; Robinson, B. A.; Hyman, J. M.; Higdon, D. Accelerating Markov Chain Monte Carlo Simulation by Differential Evolution with Self-Adaptive Randomized Subspace Sampling. *Int. J. Nonlinear Sci. Numer. Simul.* **2009**, *10* (3), 273–290. https://doi.org/10.1515/IJNSNS.2009.10.3.273.

(2) Sivia, D. S.; Webster, J. R. P. The Bayesian Approach to Reflectivity Data. *Phys. B Condens. Matter* **1998**, *248* (1–4), 327–337. https://doi.org/10.1016/S0921-4526(98)00259-2.

(3) Nielander, A. C.; Mcenaney, J. M.; Schwalbe, J. A.; Baker, J. G.; Blair, S. J.; Wang, L.; Pelton, G.; Andersen, S. Z.; Enemark-rasmussen, K.; Viktor, C.; Yang, S.; Bent, S. F.; Cargnello, M.; Kibsgaard, J.; Vesborg, P. C. K.; Chorkendor, I.; Jaramillo, T. F. A Versatile Method for Ammonia Detection in a Range of Relevant Electrolytes via Direct Nuclear Magnetic Resonance Techniques. *ACS Catal.* **2019**, *9*, 5797–5802. https://doi.org/10.1021/acscatal.9b00358.

(4) Rafaja, D.; Köstenbauer, H.; Mühle, U.; Löffler, C.; Schreiber, G.; Kathrein, M.; Winkler, J. Effect of the Deposition Process and Substrate Temperature on the Microstructure Defects and Electrical Conductivity of Molybdenum Thin Films. *Thin Solid Films* **2013**, *528*, 42–48. https://doi.org/10.1016/j.tsf.2012.06.087.

(5) Sažinas, R.; Andersen, S. Z.; Li, K.; Saccoccio, M.; Krempl, K.; Pedersen, J. B.; Kibsgaard, J.; Vesborg, P. C. K.; Chakraborty, D.; Chorkendorff, I. Towards Understanding of Electrolyte Degradation in Lithium-Mediated Non-Aqueous Electrochemical Ammonia Synthesis with Gas Chromatography-Mass Spectrometry. *RSC Adv.* **2021**, *11* (50), 31487–31498. https://doi.org/10.1039/D1RA05963G.

(6) Zhuang, G. R.; Wang, K.; Chen, Y.; Ross, P. N. Study of the Reactions of Li with Tetrahydrofuran and Propylene Carbonate by Photoemission Spectroscopy. *J. Vac. Sci. Technol. A Vacuum, Surfaces, Film.* **1998**, *16* (5), 3041–3045. https://doi.org/10.1116/1.581475.

(7) Aurbach, D.; Daroux, M. L.; Faguy, P. W.; Yeager, E. Identification of Surface Films Formed on Lithium in Dimethoxyethane and Tetrahydrofuran Solutions. *J. Electrochem. Soc.* **1988**, *135* (8), 1863–1871. https://doi.org/10.1149/1.2096170.

(8) Koch, V. R. Reactions of Tetrahydrofuran and Lithium Hexafluoroarsenate with Lithium. *J. Electrochem. Soc.* **1979**, *126* (2), 181–187. https://doi.org/10.1149/1.2129002.

(9) Kent, M. S.; Smith, G. S.; Baker, S. M.; Nyitray, A.; Browning, J.; Moore, G.; Hua, D. W. The Effect of a Silane Coupling Agent on Water Adsorption at a Metal/Polymer Interface Studied by Neutron Reflectivity and Angle-Resolved X-Ray Photoelectron Spectroscopy. *J. Mater. Sci.* **1996**, *31* (4), 927–937. https://doi.org/10.1007/BF00352892.

(10) Kienzle, P. A.; O'Donovan, K. V.; Ankner, J. F.; Berk, N. F.; Majkrzak, C. F. REFL1D.

(11) Doucet, M.; Ferraz Leal, R. M.; Hobson, T. C. Web Interface for Reflectivity Fitting. *SoftwareX* **2018**, *7*, 287–293. https://doi.org/10.1016/j.softx.2018.09.001.

(12) Wu, H.-M.; Chen, S.-A. Dopant-Polymer Interaction: MoCl5-Doped Polyacetylene. *Synth. Met.* **1988**, *26* (3), 225–236. https://doi.org/10.1016/0379-6779(88)90239-1.

(13) McIntyre, N. S.; Johnston, D. D.; Coatsworth, L. L.; Davidson, R. D.; Brown, J. R. X-Ray Photoelectron Spectroscopic Studies of Thin Film Oxides of Cobalt and Molybdenum. *Surf. Interface Anal.* **1990**, *15* (4), 265–272. https://doi.org/10.1002/sia.740150406.

(14) Colton, R. J.; Guzman, A. M.; Rabalais, J. W. Electrochromism in Some Thin-film Transition-metal Oxides Characterized by X-ray Electron Spectroscopy. *J. Appl. Phys.* **1978**, *49* (1), 409–416. https://doi.org/10.1063/1.324349.

(15) Choi, J.-G.; Thompson, L. T. XPS Study of As-Prepared and Reduced Molybdenum Oxides. *Appl. Surf. Sci.* **1996**, *93* (2), 143–149. https://doi.org/10.1016/0169-4332(95)00317-7.

(16) Biesinger, M. C. X-ray Photoelectron Spectroscopy (XPS) Reference Pages - Molybdenum http://www.xpsfitting.com/2009/10/molybdenum.html.

(17) Blair, S. J.; Nielander, A. C.; Stone, K. H.; Niemann, V.; Kreider, M. E.; Benedek, P.; McShane, E. J.; Avilés Acosta, J.; Gallo, A.; Jaramillo, T. F. Development of a Versatile Electrochemical Cell for in Situ Grazing-Incidence x-Ray Diffraction during Non-Aqueous Electrochemical Nitrogen Reduction. *Manuscr. Prep.* **2022**.

(18) Anwar, M.; Hogarth, C. A.; Bulpett, R. Effect of Substrate Temperature and Film Thickness on the Surface Structure of Some Thin Amorphous Films of MoO3 Studied by X-Ray Photoelectron Spectroscopy (ESCA). *J. Mater. Sci.* **1989**, *24* (9), 3087–3090. https://doi.org/10.1007/BF01139023.

(19) Anwar, M.; Hogarth, C. A.; Bulpett, R. An XPS Study of Amorphous MoO3/SiO Films Deposited by Co-Evaporation. *J. Mater. Sci.* **1990**, *25* (3), 1784–1788. https://doi.org/10.1007/BF01045385.